# Fukushima Daiichi Unit 1 Accident Progression Uncertainty Analysis and Implications for Decommissioning of Fukushima Reactors – Volume I

Sandia National Laboratories

# Fukushima Daiichi Unit 1 Accident Progression Uncertainty Analysis and Implications for Decommissioning of Fukushima Reactors – Volume I

Severe Accident Analysis Department – 06232
Sandia National Laboratories
P.O. Box 5800
Albuquerque, New Mexico  87185-MS0748

**Abstract**

Sandia National Laboratories (SNL) has conducted an uncertainty analysis (UA) on the Fukushima Daiichi unit (1F1) accident progression with the MELCOR code. The model used was developed for a previous accident reconstruction investigation jointly sponsored by the US Department of Energy (DOE) and Nuclear Regulatory Commission (NRC). That study focused on reconstructing the accident progressions, as postulated by the limited plant data. This work was focused evaluation of uncertainty in core damage progression behavior and its effect on key figures-of-merit (e.g., hydrogen production, reactor damage state, fraction of intact fuel, vessel lower head failure). The primary intent of this study was to characterize the range of predicted damage states in the 1F1 reactor considering state of knowledge uncertainties associated with MELCOR modeling of core damage progression and to generate information that may be useful in informing the decommissioning activities that will be employed to defuel the damaged reactors at the Fukushima Daiichi Nuclear Power Plant. Additionally, core damage progression variability inherent in MELCOR modeling numerics is investigated.

# ACKNOWLEDGEMENTS

# CONTENTS

# FIGURES

# TABLES

# ACRONYMS

| | |
|---|---|
| 1F1 | Fukushima Daiichi Unit 1 |
| 1F2 | Fukushima Daiichi Unit 2 |
| 1F3 | Fukushima Daiichi Unit 3 |
| | |
| ADS | automatic depressurization system |
| | |
| BAF | bottom of active fuel |
| BSAF | Benchmark Study of the Accident at the Fukushima Daiichi Nuclear Power Station (BSAF) Project |
| BWR | boiling water reactor |
| | |
| CDF | Cumulative Distribution Function |
| CRDHS | control rod drive hydraulic system |
| CRGT | control rod guide tube |
| CST | condensate storage tank |
| CV | control volume |
| CVH | Control Volume Hydrodynamics (package) |
| | |
| DCH | Decay Heat |
| DOE | Department of Energy |
| DW | drywell |
| | |
| FoM | Figures of Merit |
| | |
| HPCI | high-pressure coolant injection system |
| | |
| IC | isolation condenser |
| JST | Japanese Standard time |
| | |
| LPCS | low-pressure core sprays |
| | |
| MCCI | molten core concrete interaction |
| MELCOR | not an acronym |
| MOX | mixed oxide |
| MSIV | main steam-line isolation valve |
| MSL | main steam line |
| | |
| NRC | Nuclear Regulatory Commission |
| | |
| RCIC | reactor core isolation cooling system |
| RCS | reactor coolant system |
| RHR | residual heat removal system |
| RN | Radionuclide (package) |
| RPV | reactor pressure vessel |

| | |
|---|---|
| SBO | station blackout |
| SCALE6 | Standardized Computer Analyses for Licensing Evaluation |
| SNL | Sandia National Laboratories |
| SOARCA | State of the Art Reactor Consequence Analysis |
| SRV | safety relief valve |
| | |
| TAF | top of active fuel |
| TaT | Effective Fuel Failure Temperature (time-at-temperature) |
| TEPCO | Tokyo Electric Power Company |
| | |
| WW | wetwell |

# 1    INTRODUCTION

## 1.1    Background

Japan suffered an immense tragedy as a result of the 2011 Tohuku earthquake and resulting tsunami that caused widespread damage to the infrastructure of the country and more than 20,000 deaths, most from the tsunami. The magnitude 9 ($M_w$) earthquake, centered roughly 20 miles deep and 43 miles east of Japan, took place at 14:46 (JST) on March 11, 2011, and produced catastrophic damage to buildings, roads, communications, and regional electrical power. Damage to the Sendai region was especially large owing to its proximity to the epicenter of the seismic event that produced a tsunami with an estimated height that exceeded 14 meters at the site of the Fukushima reactors. The earthquake at 14:46 JST resulted in a scram and a regional loss of electrical power, requiring the Fukushima Daiichi power plants (1F1, 1F2, and 1F3) to start emergency on-site diesel powered generators to maintain cooling at the plants. 1F4 was defueled at the time for maintenance, and 1F5 and 1F6 were in a state of cold shutdown for maintenance.

The first of several tsunamis produced by the earthquake reached the Fukushima Daiichi site at roughly 15:27. At 15:46, a wave exceeding 14 meters flooded buildings resulting in the loss of emergency diesel powered AC generators and producing conditions known as Station Blackout (SBO). DC power was also lost at 1F1 and 1F2. The plants were effectively isolated from the ultimate heat sink (the ocean) due to the loss of the seawater pumps that were flooded and destroyed, and the emergency cooling systems eventually failed; each of the three units subsequently suffered core damage of varying degrees as a result of loss of water level in the reactor cores. Significant hydrogen generation resulted from the oxidation of the exposed Zircaloy fuel cladding, which occurs at elevated temperatures; this can generate heat greater than the decay heat in the fuel, and therefore may have accelerated the release of fission products from the damaged fuel to the containment vessels. With no way to reject the decay heat from the reactors, the suppression pools eventually became thermally saturated. This produced pressures in the containment vessels that eventually exceeded their design pressures. Containment venting was attempted. However, due to difficulties in accessing and operating vent valves, venting was either unsuccessful or delayed.

Ultimately, the containment systems leaked, failed, or were intentionally vented, resulting in the release of radioactivity to the reactor buildings and the environment. Combustible gasses produced from the core damage, and potentially from molten core–concrete interaction, accumulated in the 1F1 and 1F3 reactor buildings, causing explosions and destruction of portions of the buildings [2].

In response to the accident at the Fukushima Daiichi nuclear power station in Japan, the U.S. Nuclear Regulatory Commission (NRC) and Department of Energy agreed to jointly sponsor an accident reconstruction study [2] as a means of assessing severe accident modeling capability of the MELCOR code [1]. As part of that study, Sandia National Laboratories (SNL) developed MELCOR 2.1 models of the Fukushima 1F1, 1F2 and 1F3 reactors. The MELCOR models used in that study were based on the State of the Art Reactor Consequence Analysis (SOARCA) Peach Bottom BWR/4 Mk-I MELCOR model [3]. The Peach Bottom plant is a larger but quite similar in reactor design to the reactors at Fukushima. The containments are the General Electric Mk-I design where a torus-shaped suppression pool serves to prevent steam over-pressurization of the containment. The Peach Bottom MELCOR model was used as a template for developing

the Fukushima MELCOR models. Modifications were made to the Fukushima MELCOR models to include important differences in the Fukushima reactors, such as reactor dimensions, number of fuel assemblies, and operating power.

## 1.2   Purpose

The primary purpose of this work was to evaluate the influence of in-core damage progression input parameters on selected key figures-of-merit (FoMs) (e.g., fraction of failed fuel, time of lower head failure, total hydrogen produced in-core, etc.). The impetus for this is to develop a better understanding of potential plant damage states (i.e., degree of core degradation, locations of intact and degraded materials, etc.) which can in turn be used to help inform future decommissioning efforts and define areas where additional information obtained from decommissioning activities could improve understanding of severe accident progression.

In addition, in the previous 1F1 analysis [2] deviations were seen between some of the analysis results and the Tokyo Electric Power Company (TEPCO) plant data. For example, the 1F1 model predicted lower head failure between 14 and 15 hr, while the plant data pressure rise that can be postulated as indicative of lower head failure is between 11 and 12 hr. This deviation is not unexpected, as many of the parameters used in the MELCOR models that influence core degradation, and by extension, lower head failure have been developed based on a small number of separate effects tests and expert opinion; they have not been quantified with full-scale integral tests at representative boiling water reactor (BWR) station blackout (SBO) conditions.

The traditional method to perform this analysis would be to execute a series of sensitivity analyses on a set of parameters that were deemed to be important to core damage progression. While this method can potentially find a set of parameters that result in a better prediction with respect to the data, its ad hoc nature makes it difficult to quantify the sensitivity of the results to the input parameters. Given the availability of servers with hundreds of central processing unit (CPU) cores, using an uncertainty analysis approach (i.e., identifying key input parameters, accounting for uncertainty in those parameters, creating as statistically sufficient number of samples from the uncertainty distributions) to address this type of problem is much more tractable, traceable, and provides outputs that are amenable to statistical analysis.

Recent uncertainty analysis (UA) reactor analyses performed by SNL have looked at a wide range of parameters with the intent of addressing (at least to some extent) uncertainty in all phases of the accident sequence [4],[5]. For this analysis a focused set of uncertain parameters was used, specifically those associated with in-core damage progression [22]. This was done as the figures-of-merit (FoMs) of interest are directly related to in-core damage progression phase of the accident sequence.

An additional outcome of this work was the characterization of code sensitivity to the varied model inputs as well as inherent variation due to the numerical methods used in MELCOR to predict severe accident progression. The additional variability in predicted results driven by the code's inherent precision was evaluated by performing an ensemble of analyses similar to the uncertainty variations but where the range of uncertain model inputs was restricted to a relatively small span (+/- 1%). This was done to quantify the order of magnitude of the numerical precision that can be expected of complex multi-effects codes, in this case MELCOR, in the midst of broader state of knowledge variations employed in the uncertainty analysis. This characterization provides the code user with insights when assessing the magnitude of variance in the results

relative to the fundamental code precision, an important consideration when evaluating the statistical importance of the selected uncertain parameters and resulting range of potential damage states.

## 1.3   Document Outline

A summary description of the 1F1 MELCOR model is provided in Section 2. The UA approach, the characterization of the uncertain input parameter distributions, and a description of the analyses performed with the 1F1 MELCOR model are discussed in Section 3. Results from the analyses are presented in Section 4. Section 5 addresses the relevance of these uncertainty results to anticipated future decommissioning activates for the Fukushima Daiichi reactors. In Section 6 the results of a code numerical precision study are described to aid in assessing code results. Finally, summary and conclusions are presented in Section 7.

# 2    MELCOR MODEL DESCRIPTION

The 1F1 MELCOR model was originally developed from the MELCOR BWR/4 Mk-I boiling water reactor model created for the NRC's SOARCA project [3]. Care was taken during 1F1 model development to ensure that it adequately represented a BWR/3 reactor, which is a smaller reactor compared to the BWR/4 designs of 1F2, 1F3, and Peach Bottom. The SOARCA documentation [8] provides a summary description of that model. A comprehensive description of that model is also available in reference [9]. Section 3 of the Fukushima Daiichi accident study [2] contains the majority of the SOARCA model summary description along with subsections describing the implementation of Fukushima-specific information used to create the Fukushima MELCOR model.

Since the Fukushima Daiichi accident study report [2] was issued, new information on the plant geometry and the accident sequence has been provided by the Japan Atomic Energy Agency (JAEA) [10] to SNL. This new information has been incorporated into the 1F1 model that is used for this analysis.

This section will provide a brief summary of the model descriptions given in references [8] and [9], with a focus on model nodalization. In addition, an accident event timeline will be provided, along with discussions of how the timeline events were implemented into the 1F1 MELCOR model.

A review of the historical development of the BWR/4 Mk-I MELCOR model is provided in Section 2.1. A brief description of the MELCOR code is provided in Section 2.2. Section 2.3 contains a summary description of the 1F1 MELCOR model nodalization. Section 2.4 provides a discussion of the 1F1 radionuclide and decay heat characterization. A discussion of the accident event timelines and associated model modifications are given in Section 2.5. Finally, Section 2.6 provides the computational platform and code executables used for this work.

## 2.1    SNL BWR/4 Mk-I MELCOR Model History

The MELCOR SOARCA BWR/4 Mk-I model was originally created at Brookhaven National Laboratory for code assessment applications with MELCOR 1.8.0; it is based on the Peach Bottom Atomic Power Station Unit 2 Reactor design. The model was subsequently used by the Oak Ridge National Laboratory to study differences between fission product source terms predicted by MELCOR 1.8.1 and those generated for use in NUREG-1150 [18], "Severe Accident Risks: An Assessment for Five U.S. Nuclear Power Plants", using the Source Term Code Package [11]. In 2001, SNL refined the BWR/4 core nodalization to support the developmental assessment and release of MELCOR 1.8.5. These refinements concentrated on the spatial nodalization of the reactor core (in terms of fuel and structural material and hydrodynamic volumes) used to calculate in-vessel melt progression. However, the overall scope of the model also expanded to permit a wider spectrum of accident scenarios to be examined, some of which involved operation or delayed failures of plant safety systems.

These developments culminated in a model that was applied in the reassessment of radiological source terms for high burnup and mixed oxide (MOX) core designs, and a comparison of their release characteristics [12] to the regulatory prescription outlined in NUREG-1465, "Accident Source Term for Light-Water Nuclear Power Plants," issued February 1995 [13]. These

calculations addressed a wide spectrum of postulated accident sequences, which required the following new models to represent diverse plant design features:

- modifications of features needed to achieve steady-state reactor conditions (e.g., recirculation loops, jet pumps, steam separators, steam dryers, feedwater flow, control rod drive hydraulic system (CRDHS), main steam lines, turbine/hotwell, core power profile),

- new models and control logic to represent coolant injection systems (e.g., RCIC, HPCI, residual heat removal system (RHR), and low-pressure core sprays (LPCS)) and supporting water resources (e.g., condensate storage tank (CST) with switchover), and

- new models to simulate reactor vessel pressure management (e.g., safety relief valves (SRVs), safety valves, automatic depressurization system (ADS), and logic for manual actions to affect a controlled depressurization if torus water temperatures exceed the heat capacity temperature limit).

Subsequent work in support of other NRC research programs motivated further refinement and expansion of the Peach Bottom MELCOR model in two broad areas. The first area focused on the spatial representation of primary and secondary containment. The drywell portion of primary containment has been subdivided to distinguish thermodynamic conditions internal to the pedestal from those within the drywell itself. Refinements have also been made to the spatial representation and flow paths within the reactor building (i.e., secondary containment). The second area has focused on bringing the model up to current best practice standards for MELCOR 1.8.6 [14].

The SOARCA BWR/4 Mk-I MELCOR model was chosen as the starting point for the development of the Fukushima reactor models, as it is the current state-of-the-art BWR/4 Mk-I MELCOR model. At Fukushima Daiichi, Units 2 and 3 are BWR/4 reactors, while Unit 1 is of a very similar reactor design (BWR/3). Furthermore, Units 1, 2, and 3 all have the Mk-I containment design.

## 2.2  MELCOR Computer Code Description

MELCOR [1] is a fully integrated, engineering-level computer code that models the progression of severe accidents in light-water reactor nuclear power plants. MELCOR is being developed at Sandia National Laboratories for the U.S. NRC as a second-generation plant risk assessment tool and the successor to the Source Term Code Package [11]. A broad spectrum of severe accident phenomena in both boiling and pressurized water reactors is treated in MELCOR in a unified framework. These include thermal-hydraulic response in the reactor coolant system (RCS), reactor cavity, containment, and confinement buildings; core heatup, degradation, and relocation; core-concrete attack; hydrogen production, transport, and combustion; fission product release; and transport behavior. Figure 2.1 illustrates the wide range of processes and phenomena during a severe accident that are modeled in the MELCOR code.

Current uses of MELCOR include estimation of severe accident source terms and their sensitivities and uncertainties in a variety of applications.
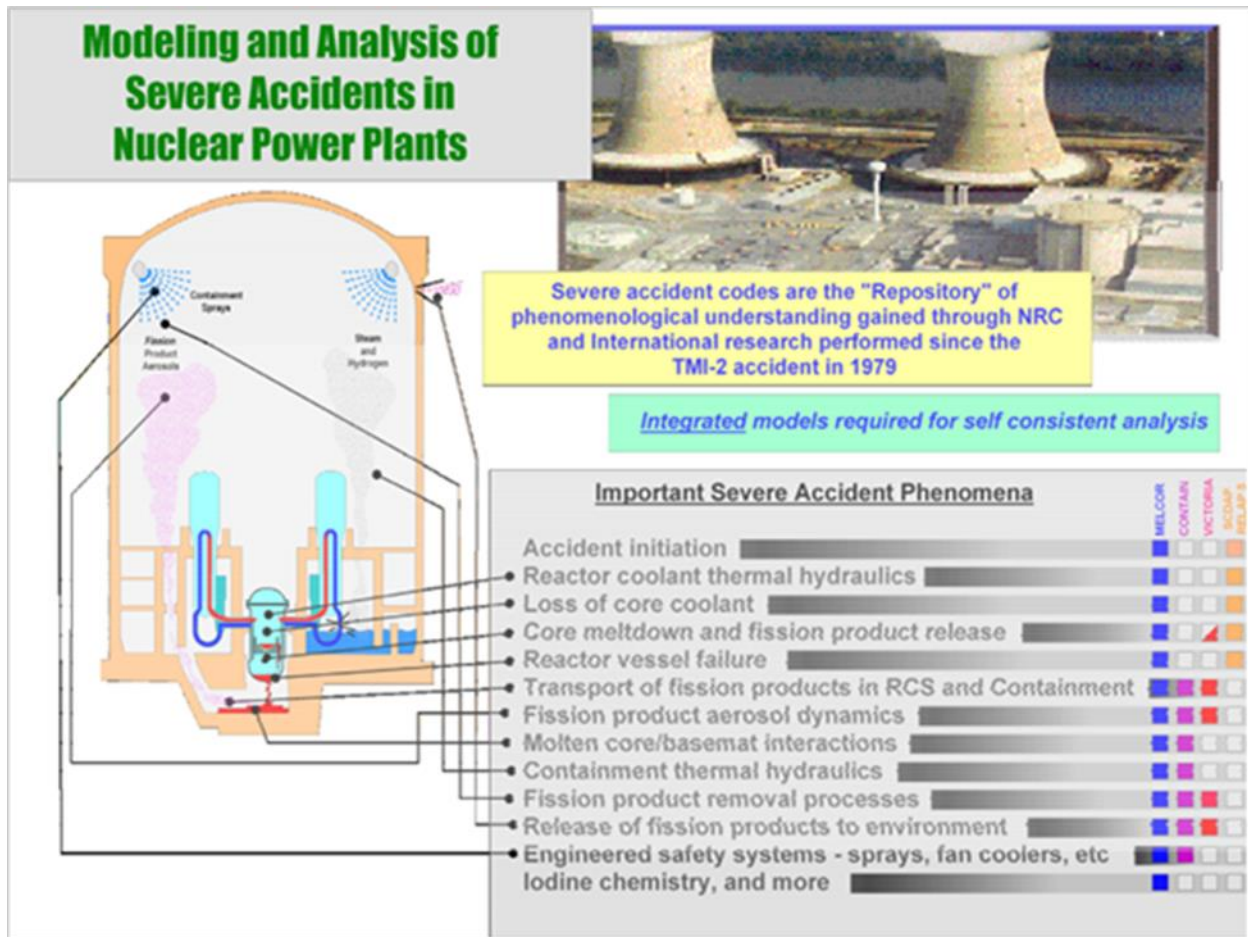
**Figure 2.1 – Illustration of the Range of Phenomena and Processes Modeled in the MELCOR Accident Analysis Code.**

## 2.3  1F1 MELCOR Model Nodalization

The RPV nodalization in the 1F1 model is similar to that in the Peach Bottom SOARCA model [9] and the 1F1 model in [2]. Changes were made to the nodalization to make it consistent with the RPV nodalization in the JAEA data set [10]. This alignment simplifies the processing of the JAEA data into MELCOR input (e.g., control volume elevations, control volume free volumes, etc.).

Excluding the core region, the reactor pressure vessel is broken up into the following control volumes (CVs) (see Figure 2.2). Note that while control volumes define the spatial domain of the MELCOR analysis, the control volumes are connected with MELCOR "Flow Paths" which define the flow network that allows the flow and exchange of hydrodynamic materials such as water, steam and hydrogen:

- lower plenum (CV_320)

- jet pumps (CV_300)

- lower downcomer (CV_312)

- upper downcomer (CV_314)

- upper core shroud (CV_345)

- steam separators (CV_350)

- steam dome (CV_360)

Flowpaths (FL) connect the RPV CVs:

- steam dome-to-upper downcomer (FL_360-314)

- upper downcomer-to-lower downcomer (FL_314-312)

- lower downcomer-to-jet pumps (FL_312-300)

- jet pumps-to-lower plenum (FL_300-320)

- upper core shroud-to-steam separators (FL_345-350)

- steam-separators-to-steam dome (FL_350-360)

- steam-separators-to-upper downcomer (FL_350-314)

Also, not shown, are the FLs that connect the lower plenum to the channel and bypass CVs at the bottom of the core (one FL per homogenized region of the core {COR ring}) and that connect the channel and bypass CVs at the top of the core to the upper core shroud CV (one FL per COR ring).

The heat structures (HS) (shown in various shades of orange in Figure 2.2) that represent the RPV vessel are

- hemispherical portion of steam dome CV (HS_360-200.2)

- cylindrical portion of steam dome CV (HS_360-200.1)

- cylindrical portion of upper downcomer CV (HS_314-200)

- cylindrical portion of lower downcomer CV (HS_312-200)

The heat structures below the core shroud are

- core shroud support structures (HS_320-320)

- lower downcomer/lower plenum wall (HS_320-312)

The core shroud heat structures are

- one HS at each core axial level from level 5 to level 17 (HS_xxx-yyy_zz), where xxx is the CV# of the CV inside the core shroud, yyy is the CV# of the CV outside the core shroud, and zz is an the index number that differentiates HS for different core axial levels that are associated the same inside and outside CVs.

The upper core shroud is represented by two heat structures

- cylindrical portion of the upper core shroud (HS_345-312.1)

- domed portion of the upper core shroud (HS_345-312.2)

The steam separators are represented by three heat structures

- the standpipes (HS_350-314.1)

- the portion of the separators within the upper downcomer CV (HS_350-314.2)

- the portion of the separators within the steam dome CV (HS_350-360)

Note that the lower head is not treated as a heat structure, rather it modeled in MELCOR as part of the COR package.

In addition, there are CVs, FLs, and HSs that represent the four main steam lines and the two recirculation pump loops (not shown in Figure 2.2). Note that Heat Structures (HS), another MELCOR input component define physical elements of the reactor and containment such as the mass of steel in RCS piping or the walls of the containment and reactor building. Heat structures can absorb (store) or transfer heat by conduction, convection or radiation process considered in the MELCOR time-step advancement.

Figure 2.3 shows the both the COR and CV/FL nodalization of the core. In the COR package, the core is modeled with 6 rings and 17 axial core levels. The axial levels are comprised

- level 1: control rod stub tubes (CRSTs)

- level 2-5: control rod guide tubes (CRGTs)

- level 6: lower core plate, lower tie, plate, nose pieces, and "Elephant's Foot"

- level 7-16: fuel, control blades, and canisters

- level 17: top guide and upper tie plate

Note that while there are ring 6 COR cells in axial levels 2-5, there are no core materials in those cells.

The COR cells in axial levels 1-6 are associated with the lower plenum (CV_320). In core region above the lower core plate/lower plenum there are 5 channel and 5 bypass CVs (arrayed axial) in each ring. Two axial COR cells are associated with a corresponding CV (as shown in Figure 2.3), with the exception of the top-most CVs which are associated with 3 COR cells.
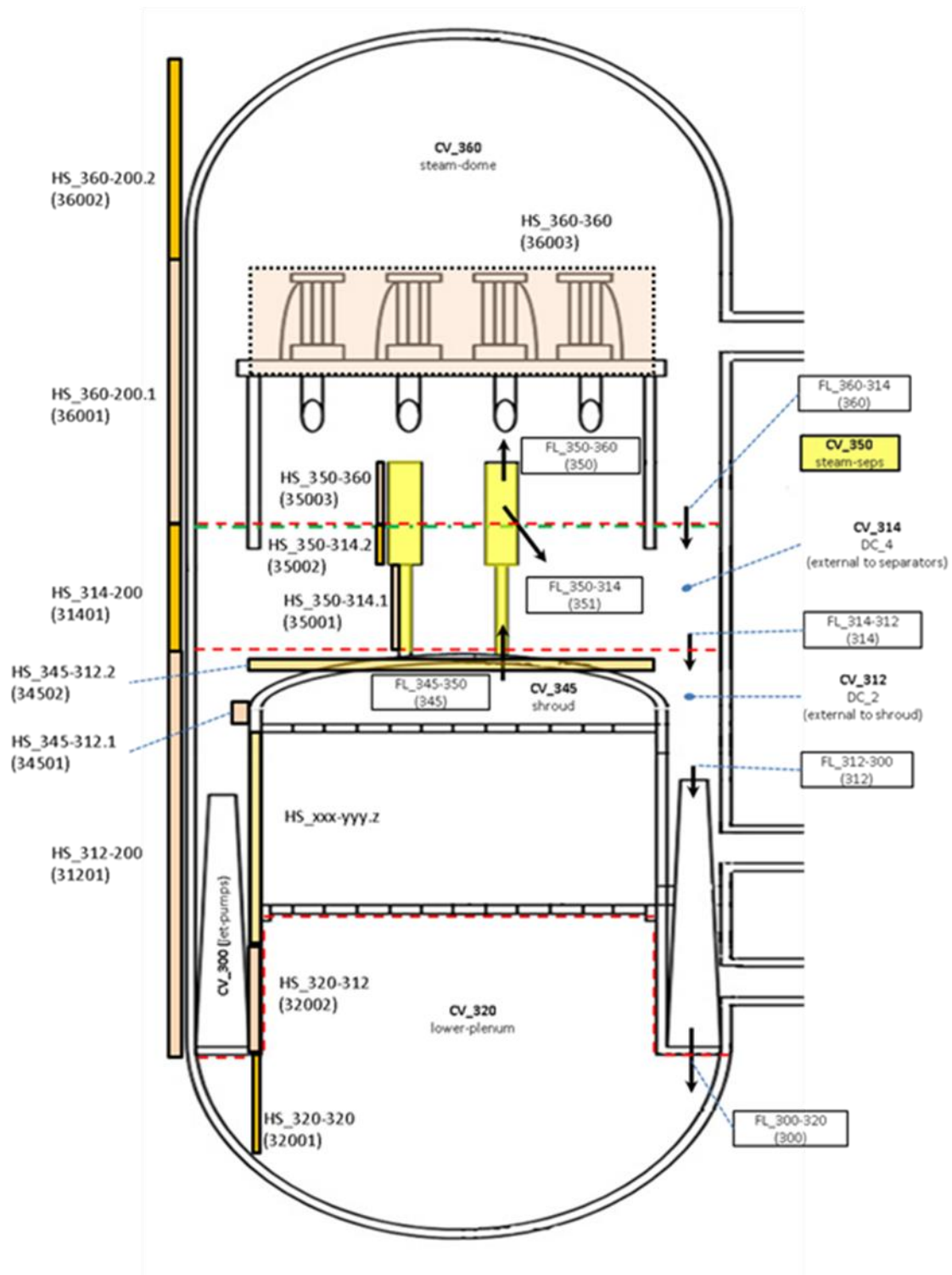
**Figure 2.2 – Reactor Pressure Vessel Nodalization**

**Figure 2.3 – Core Nodalization showing control volume and fuel/component discretization used to characterize the reactor core.**

11

The primary containment of the Mk-I design consists of two separate regions: a drywell (DW) and a wetwell (WW) (see Figure 2.4). The drywell is divided into two CVs, one for the region within the pedestal under the RPV (CV205) and one for the balance of the drywell (CV200). The wetwell is also divided into two CVs, one for the drywell steam vents that connect the drywell to the torus (CV210), and one for the torus itself (CV220). Previous analyses have used multiple CVs for the torus, both in terms of dividing it into separate atmosphere and pool CVs, as well as dividing it into multiple radial segments. These multiple-CV implementations are done as an attempt to model the thermal gradients that occur due to a single SRV venting into one region of the torus. The concept of modeling the thermal stratification thought to occur in the suppression pool is a topic of current intense study and when this phenomena becomes better understood, the effects will be included in equivalent MELCOR nodalization that would capture this effect, informed by new experimental data or other detailed code analyses (CFD for example). For now, we neglect this effect in the current analyses.
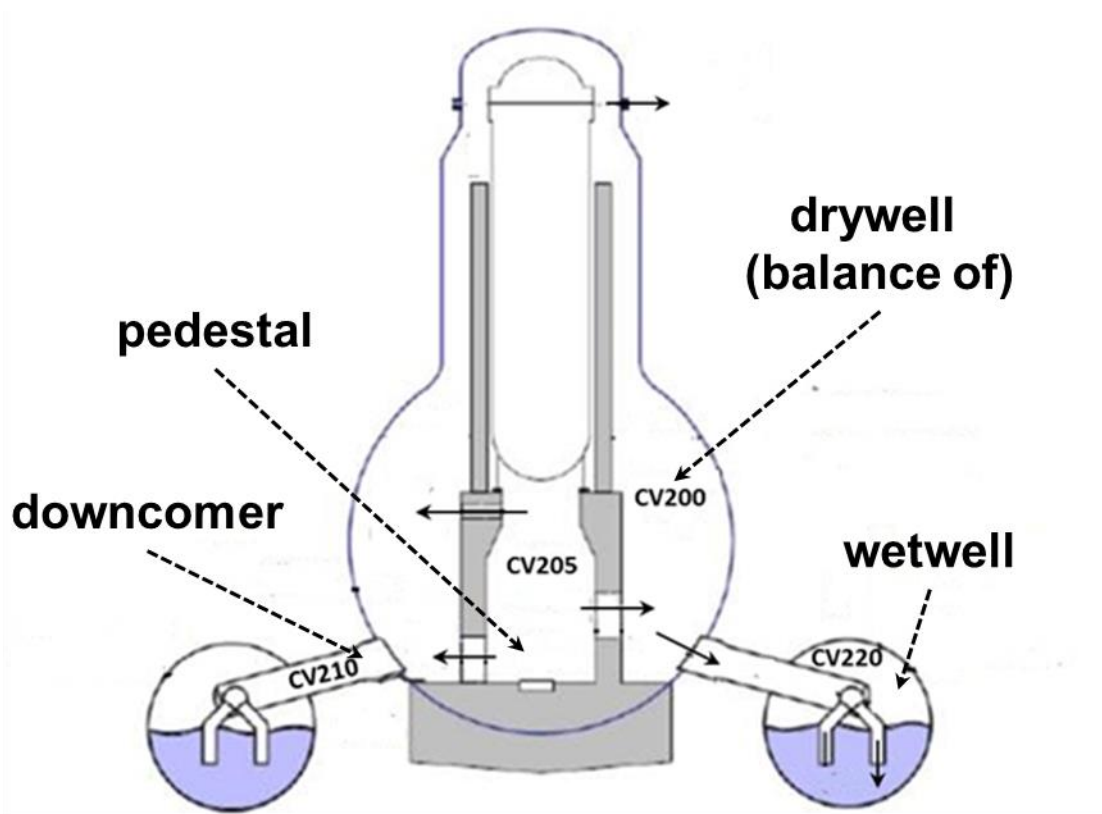


**Figure 2.4 – Containment Nodalization showing drywell and wetwell compartments.**

## 2.4   1F1 Radionuclide Inventory and Decay Heat Characterization

The SNL MELCOR model for 1F1 implements consistent lumped radionuclide (RN) class inventories and class powers, total core decay power, and nuclide-level inventories (for MACCS) that are generated from the SCALE6 code package [19]. The pertinent MELCOR and MACCS input records are derived directly from SCALE6 burnup calculations in a fully automated fashion. In particular, ORIGEN-S is used in conjunction with the Automatic Rapid Processing (ARP) module for problem-dependent cross sections. ARP estimates problem-dependent cross

sections by interpolating between data libraries available at discrete levels of enrichment, burnup, and void fraction. ORIGEN-S/ARP outputs are processed automatically by Perl scripts to directly create MELCOR inputs of RN class inventories, class specific decay powers, and total core decay power. Concurrently, MELMACCS inputs for nuclide inventories are written to enable MACCS to breakdown the MELCOR source term into isotopic releases. The isotopic inventories are entirely consistent with the lumped RN inventories specified in MELCOR, since all of the information is derived from the same ORIGEN-S calculations. A comprehensive description of the ORIGEN-S/ARP analyses of Fukushima and the post-processing methods used to create MELCOR/MACCS inputs is provided by [15].

The current MELCOR inputs are derived from calculations that make use of the pre-generated, collapsed data libraries available in SCALE6 that are based on TRITON [19] calculations with ENDF-B/V cross sections; these cross section libraries are used in conjunction with decay data from ENDF-B/VII.1 for the calculation of the MELCOR and MACCS inputs. The surrogate BWR cross section libraries in SCALE6 are reasonably representative of the Fukushima reactors for the purposes of lumped RN class inventories and decay heating, and are more than adequate for uncertainty analyses that concentrate on severe accident phenomena such as core degradation. However, in anticipation of future source term analyses, SNL has recently completed TRITON modeling efforts to generate data libraries for each of the fuel assembly types in units 1-3 at Fukushima. These new libraries make use of the latest ENDF-B/VII.1 cross sections and are more representative of the Fukushima fuel than the pre-generated ENDF-B/V libraries. Accurate data libraries are necessary for best-estimate inventories in source term analyses, particularly for certain actinides ($^{238}$Pu, $^{241}$Pu) and neutron absorption products ($^{134}$Cs) that are important for health effects. Fukushima research on source term quantification will utilize updated SCALE6 calculations that make use of the detailed fuel assembly models and data libraries.

The ORIGEN-S/ARP models use plant-specific core design and operating history information from TEPCO [20]. This includes power and burnup distributions, the number of previous irradiation and decay cycles, enrichments, void fraction distributions, overall thermal power and fuel loading, and the time of shutdown in the last operating cycle. The types of fuel assemblies, such as the details of fuel lattice (i.e., 8x8, 9x9, etc.) and water rod size/placement, are treated by the ARP libraries that are generated by TRITON.

## 2.5   Accident Event Timeline

Table 2.1 lists the key events in the 1F1 accident sequence [2]. For this analysis the model is only run to the time at which fresh water injection was started (15 hr) as results beyond this time are not relevant for the purpose of this report.

Information provided in [17] indicates that the main steam isolation valves did not start to close until 52.5 s, and were not fully closed until 55.5 s. These values, with a linear closure rate, were implemented into the main steam isolation valve (MSIV) control logic in the 1F1 model.

Reference [17] also provided a feedwater flow rate for the time from scram and when the feedwater pump halted. This feedwater flow rate time-history was implemented into the feedwater flow rate control logic in the 1F1 model (see Figure 2.5).

13

**Table 2.1 – 1F1 Event Timeline**

| Date and time | Time after scram (hr) | Event |
|---|---|---|
| 3/11 14:46 | 0.00 | Earthquake; reactor scrammed; feedwater pump coast-down |
| 3/11 14:47 | 0.014583 to 0.0154167 (52.5 to 55.5 s) | MSIVs close |
| 3/11 14:52 | 0.10 | Isolation Condensers (ICs) automatically starts (Train A and B) |
| 3/11 15:03 | 0.28 | Isolation Condensers (Train A and B) manually stopped to control cool down rate |
| 3/11 15:17 | 0.52 | Isolation condenser train A manually started |
| 3/11 15:19 | 0.55 | Isolation condenser train A manually stopped |
| 3/11 15:24 | 0.63 | Isolation condenser train A manually started |
| 3/11 15:26 | 0.67 | Isolation condenser train A manually stopped |
| 3/11 15:27 | 0.68 | First tsunami wave hits |
| 3/11 15:32 | 0.77 | Isolation condenser train A manually started |
| 3/11 15:34 | 0.80 | Isolation condenser train A manually stopped |
| 3/11 15:35 | 0.82 | Second tsunami wave hits |
| 3/11 15:41 | 0.92 | Station Blackout |
| 3/11 18:18 | 3.53 | Isolation condenser train A manually started (not implemented in the model) |
| 3/11 18:25 | 3.65 | Isolation condenser train A manually stopped (not implemented in the model) |
| 3/11 21:30 | 6.73 | Isolation Condenser train A manually started (not implemented in the model) |
| 3/12 5:46 | 15.00 | Fresh water injection from fire water pump starts End of simulation |
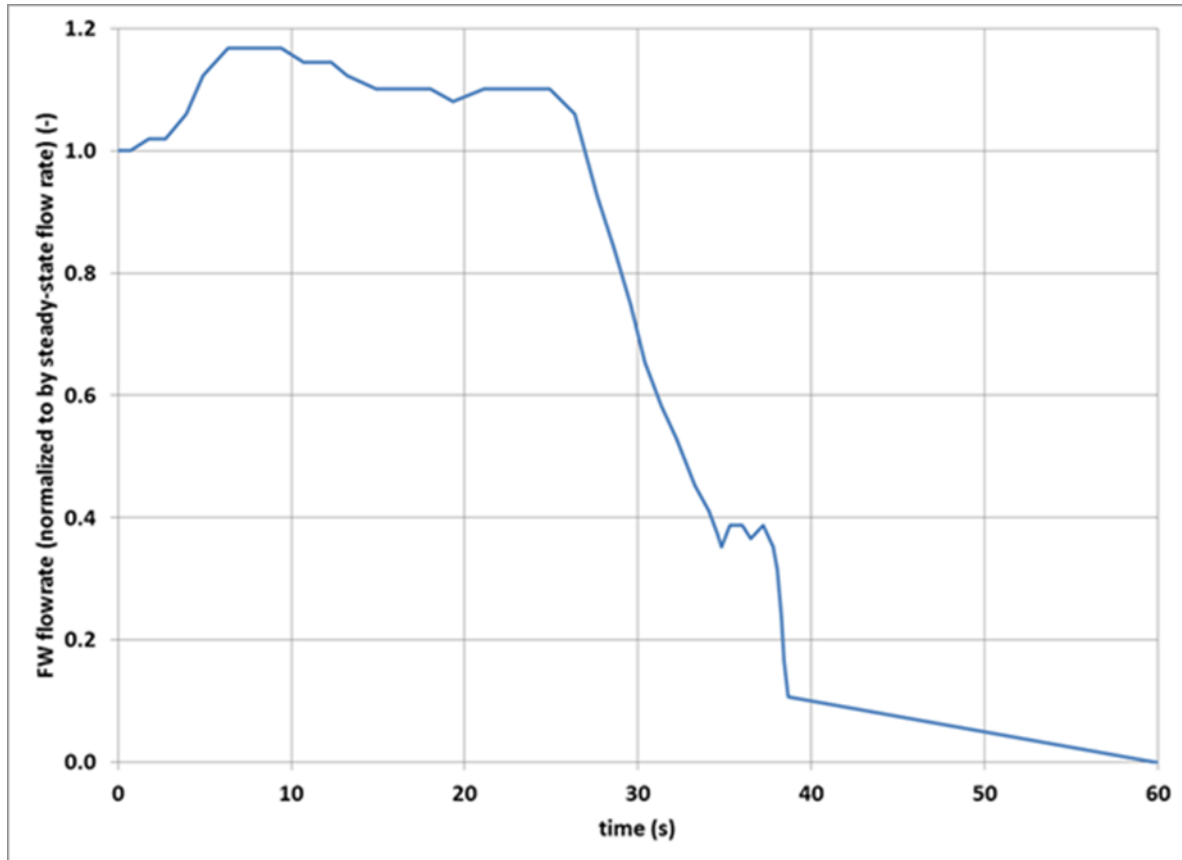
**Figure 2.5 – Normalized feedwater coast-down curve**

The 1F1 reactor is equipped with isolation condensers (IC's). These isolation condensers reside in the upper reactor building and consist of a shell and tube heat exchanger that condenses primary system steam, rejecting heat to the shell side of the condenser. Motor operated valves must be manually opened in order for steam to flow to the condenser and for condensed water to return to the RPV. Each IC has a rated capacity of 42.2 MW [17]. The capacity is calculated by multiplying the rated capacity by a pressure-based utility factor [16] (see Table 2.2) to account for the decrease in IC efficiency at lower pressures. In the model, a simple negative energy source function (equal to the 42.2 MW times the utility factor times the number of ICs operating) is used to simulate the operation of the ICs.

**Table 2.2 – IC Utility Factor**

| Pressure (Pa) | utility factor (-) |
|---|---|
| 3.26E+06 | 0.12 |
| 4.13E+06 | 0.33 |
| 5.07E+06 | 0.55 |
| 6.15E+06 | 0.80 |
| 7.24E+06 | 1.00 |

Also, the IC operation as specified by the 1F1 timeline was modified. For the last two operating periods (3.53 – 3.65 hr; 6.73 – 20.23 hr), IC operations were not included in the analysis due to the brevity of the first operation period and the model prediction of RPV depressurization prior to the last operation of the IC. Furthermore, the presence of non-condensable gases and aerosols (as predicted by the MELCOR model) is assumed to largely disable the ICs' functionality. This treatment is consistent with the current OECD-NEA BSAF 1F1 characterization of the IC operation [17].

## 2.6   Computational Platform and Code Version

The MELCOR models were executed on an SNL Windows server cluster:

DEF Cluster, 66 nodes, total of 264 cores
Hyperthreading NOT enabled
Dell PowerEdge 2950 server (dual processors)
OS: Windows Enterprise Server 2003
Xeon 5160, 3.0 GHz 2-core (no turbo), 4 MB L2 cache, 80 W max TDP
8GB RAM/System

All of the MELCOR analyses were run with MELCOR 2.1 version 5864 using the following executables:

- Melgen_RL_NL_5864.exe

- Melcor_RL_NL_5864.exe

# 3 MELCOR ANALYSIS

This section discusses the 1F1 MELCOR cases that were run for the UA. A summary of the uncertain parameters used in the analysis is given in Section 3.1. The methodology used to execute the UA cases is Section 3.2.

## 3.1 Uncertain Modeling Parameters

A scoping study was performed to make a preliminary selection of uncertain parameters for this UA [22]. Based on that work, a final set of uncertain parameters (see Table 3.1) were selected and characterized (see Section 2 of [23]) for use in this analysis. The selection of uncertain model parameters for the most part were chosen based on prior experience in previously conducted uncertainty quantification studies (eg. SOARCA Peach Bottom – reference 4 and 5) where the focus was on parameters thought to affect core melt progression and hydrogen generation. SNL improved on the technical justifications for these parameters, ranges and distributions [24]. While the details on these justifications and distributions will not be repeated here, the selected parameters are known to affect timing of cladding failure, fuel rod failure, extent of hydrogen generation, melt relocation in core (radial and lateral spreading) and re-freezing behavior of draining molten core materials. These are summarized in Table 3.1.

In addition to model parameters, decay heat is also known to be a significant uncertain parameter that affects coolant boildown rates and uncovered fuel/cladding heatup rates. This uncertainty was also included where Figure 3.1 shows the decay heat time history curves that were developed from a series of SCALE6 [19] analyses informed by ANS-5.1 [24] time-dependent decay heat uncertainties. The details of how the decay heat time history curves were developed is discussed in Section 2.2.2 of [23] and in [15]. Out of the 30,000 decay heat time history curves created a set of size 100 was randomly selected.

The "time-at-temperature" fuel rod failure treatment is a fairly recent modeling best practice developed in the SOARCA analyses to address cliff-edge behaviors in fuel rod collapse that were formerly treated as temperature threshold criteria. The time at temperature treatment, similar to a Larsen miller or other lifetime model approaches introduces a smoothness to rod failure prediction that mitigates undesired bifurcation tendencies of a simple failure threshold failure approach. Simply stated, fuel that experiences a lower time-temperature integral will collapse at a later time that fuel that experiences a larger time-temperature integral, ensuring that eventually either will fail in time and unphysical bifurcations where one zone might fail and another never fail are avoided. The methodology used to characterized time-at-temperature uncertainty is described in Section 2.2.3 of [23]. The mean, median, 10th percentile, and 90th percentile time-at-temperature curves, along with the time-at-temperature curve from the SOARCA analysis [8] are shown in Figure 3.2. Out of the 27725 time-at-temperature curves created as set of size 100 was randomly selected.

**Table 3.1 – State of Knowledge Uncertain Parameters**

| Parameter | Nomenclature | Shifted Beta Distribution (Mode/Mean) |
|---|---|---|
| time constants for radial (solid) debris relocation | SC1020_1 | LB = 180 s<br>UB = 720 s<br>$\alpha$ = 1.33<br>$\beta$ = 1.67 |
| time constants for radial (liquid) debris relocation | SC1020_2 | LB = 30 s<br>UB = 120 s<br>$\alpha$ = 1.33<br>$\beta$ = 1.67 |
| d$T$/d$z$ model[1], time constant for averaging hydrodynamic material flows | SC1030_2 | LB = 0.09 s<br>UB = 0.11 s<br>$\alpha$ = 1.1<br>$\beta$ = 1.1 |
| d$T$/d$z$ model, characteristic time for coupling d$T$/d$z$ temperatures to average CVH volume temperature when d$T$/d$z$ model is active | SC1030_4 | LB = 8 s<br>UB = 12 s<br>$\alpha$ = 1.1<br>$\beta$ = 1.1 |
| d$T$/d$z$ model, maximum relative weight of old flow in smoothing algorithm involving time constant for averaging flows | SC1030_5 | LB = 0.5 s<br>UB = 0.7 s<br>$\alpha$ = 1.1<br>$\beta$ = 1.1 |
| molten zircaloy melt break-through temperature | SC1131_2 | LB = 2100 K<br>UB = 2540 K<br>$\alpha$ = 2.77<br>$\beta$ = 2.33 |
| molten cladding (pool) drainage rate | SC1141_2 | LB = 0.1 kg/m-s<br>UB = 2.0 kg/m-s<br>$\alpha$ = 1.11111<br>$\beta$ = 1.8889 |
| fraction of strain at which lower head failure occurs | SC1601_4 | LB = 0.16<br>UB = 0.20<br>$\alpha$ = 1.1<br>$\beta$ = 1.1 |
| scaling factor for candling heat transfer coefficients | cor_cht_hfzrXX | LB = 0.9<br>UB = 1.1<br>$\alpha$ = 1.1<br>$\beta$ = 1.1 |

---

[1]  The dT/dz model is a subgrid model used in MELCOR to estimate axial temperature gradients in hydrodynamic flow (e.g. steam) to account for gas heatup over the axial extent of an otherwise lumped temperature predicted for the control volume. The purpose of the dT/dz model is to improve estimated for heat transfer from rods to flowing gas within a given control volume.

**Table 3.1– State of Knowledge Uncertain Parameters , Cont.**

| Parameter | Nomenclature | Shifted Beta Distribution (Mode/Mean) |
|---|---|---|
| fraction of un-oxidized cladding thickness at which thermal-mechanical weakening of oxidized cladding begins | cor_rod_2 | LB = 0.0005 m<br>UB = 0.0015 m<br>$\alpha = 1.1$<br>$\beta = 1.1$ |
| debris quenching heat transfer coefficient to pool | cor_lp_2 | LB = 100 W/m$^2$ K<br>UB = 2000 W/m$^2$ K<br>$\alpha = 1.1$<br>$\beta = 1.1$ |
| debris falling velocity | cor_lp_4 | LB = 0.01 m/s<br>UB = 1.0 m/s<br>$\alpha = 0.85$<br>$\beta = 1.14$ |
| minimum debris porosity (Lipinski dryout model); SC1244(1)<br>min. porosity used in flow blockage Ergun pressure drop equation; SC4413(5)<br>min. hydrodynamic volume fraction; SC4414(1)<br>minimum porosity to be used in calculating the flow resistance in the flow blockage model; SC1505(1)<br>minimum porosity to be used in calculating the area for heat transfer to fluid; SC1505(2)[2] | minpordp | LB = 0.01<br>UB = 0.2<br>$\alpha = 1.1$<br>$\beta = 1.1$ |

**Table 3.1– State of Knowledge Uncertain Parameters , Cont.**

| Parameter | Nomenclature | Uniform Distribution | Shifted Beta Distribution (Mode/Mean) |
|---|---|---|---|
| Fuel rod time-at-temperature relationship[3] | TaT | n/a | n/a |
| Time dependent core decay heat[4] | dch | n/a | n/a |

---

[2] Minimum debris porosity is defined in many locations of the MELCOR input. For consistency, the same distribution and subsequent sampled values are applied to each sensitivity coefficient.

[3] Fuel rod time-at-temperature and Time dependent decay heat are tabular uncertain variables, not point estimates. See the appropriate section for more information regarding the characterization of these variables.

[4] Fuel rod time-at-temperature and Time dependent decay heat are tabular uncertain variables, not point estimates. See the appropriate section for more information regarding the characterization of these variables.
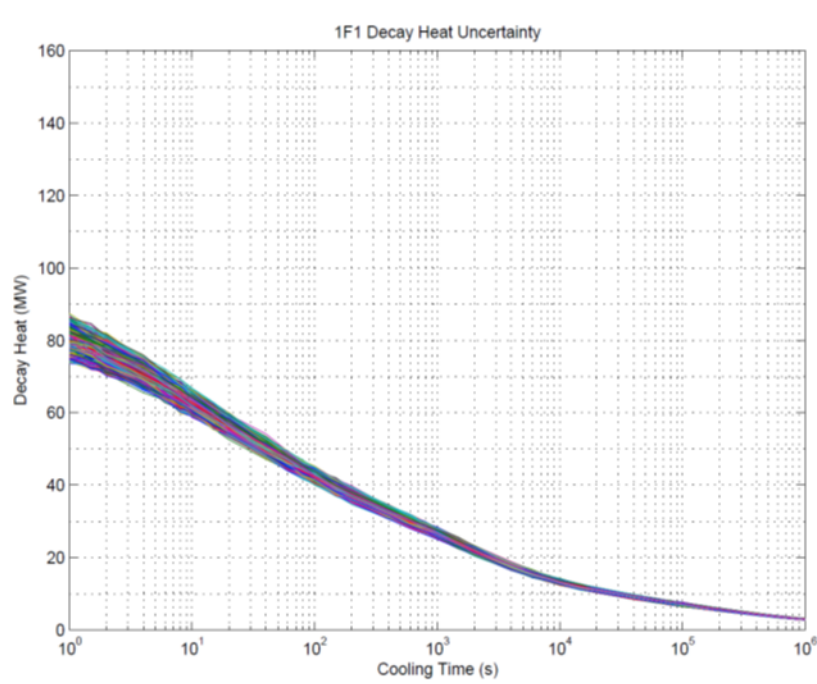
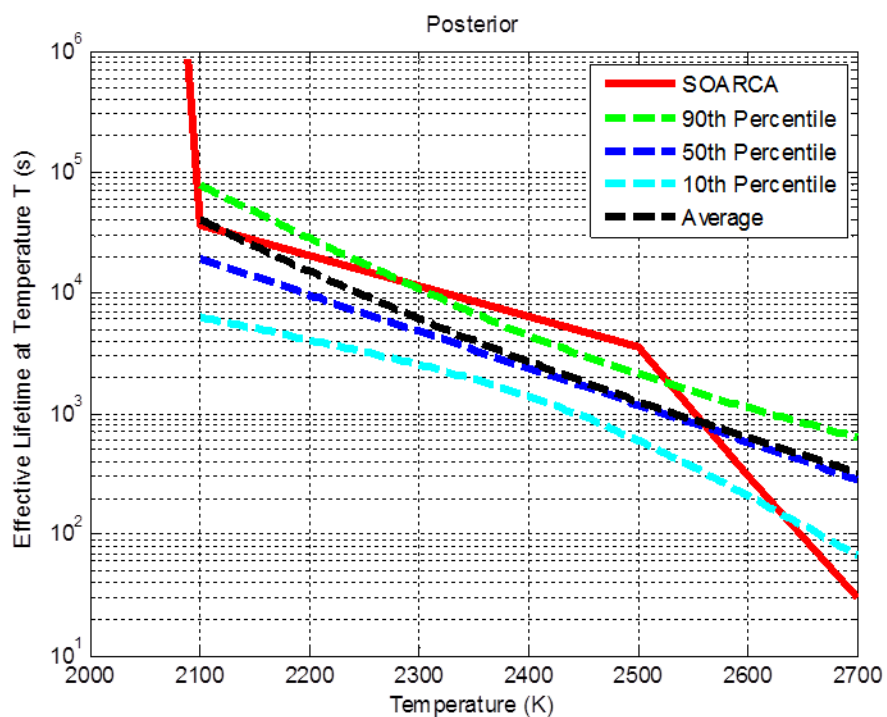**Figure 3.1 – Fukushima 1F1 Decay Heat Time History Curves**



**Figure 3.2 – Statistical Representation of Shark-Fin Failure Curves Overlaid on the SOARCA [4] Time at Temperature Failure Curve**

## 3.2  UA Execution

Figure 3.3 shows elements and processes used to perform the MELCOR calculations for the UA.

- The 1F1 MELCOR input deck and the uncertain parameters are combined into the input template for the MELCOR Uncertainty Engine software.

- The MELCOR Uncertainty Engine software is run, producing "N" MELCOR input files (where "N" is the number of realizations; for these analyses N = 100).

- Pre-sampled files of Decay Heat tables and Time-at-Temperature tables are added to the MELCOR input file set.

- Each realization is run using MELGEN/MELCOR. The runs were executed on an SNL Windows server cluster; a set of MELCOR output files is generated by each realization's execution.
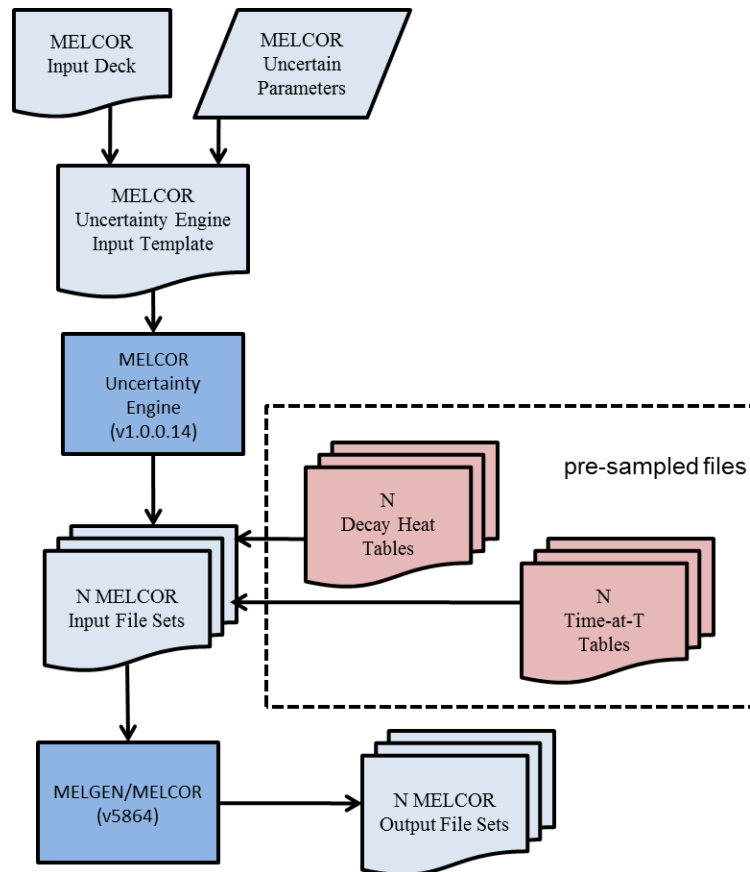


**Figure 3.3 – Diagram of Information Flow of the 1F1 Uncertainty Analysis**

# 4     RESULTS OF MELCOR UNCERTAINTY ANALYSIS

A statistical analysis of these uncertainty analysis cases and other "perturbation case" results is documented and discussed in reference [23] which describes more on methodology, statistical importance of selected uncertain parameters and tests of statistical convergence. The remainder of this report describes the uncertainty ranges of the selected fissured of merit and discusses their significance to severe accident modeling and to anticipated Fukushima reactor decommissioning activities.

## 4.1     Overview and General Observations

Horsetail plots[5] with the statistical median (red) and median-like realization (rlz13) (green) are given for the following figures-of-merit:

### 4.1.1  Primary System Pressure Response

Shown in Figure 4.1 is the spectrum of predicted RPV pressure histories for the 100 realizations examined in this study.  Initially, the RPV pressure shows a large drop due to the delay between scram and closure of the MSIVs. It then undergoes a series of increases when the ICs are not running and decreases during IC operation. During this time the individual realization pressure plots all nearly converge to the median value. This shows that the uncertainty (as characterized in this analysis) in decay heat (the only uncertain parameter that is in effect over this time period) has little to no effect on the RPV pressure during this time period.

Once the ICs are no longer operated (0.8 hr) due to loss of function on arrival of the tsunami, the cycling of a single, low set-point SRV causes RPV pressure to oscillate between the SRV open and close values between about 7.3 and 7.7 MPa.

The sudden drop in pressure predicted for all realizations between about 4 and 5.2 hours is due to a predicted rupture of the main steam line associated with high core exit gas temperature elevated RPV pressure (i.e., a Laron Miller creep rupture).  Also, RPV water level begins to decrease as water inventory is vented from the RPV to the WW by the SRV. During this time-period the SRV open and close times begin to vary, which causes the RPV pressure to vary between realizations.

---

[5] A horsetail plot is a time vs. dependent parameter plot of all of the realizations for a given case (i.e., a 100 realization plot of total hydrogen generation would have 100 time-history curves. Typically the individual realizations are plotted as thin, light grey lines, while statistical measures (e.g., median, mean, percentiles) are overlaid with thicker, colored lines.
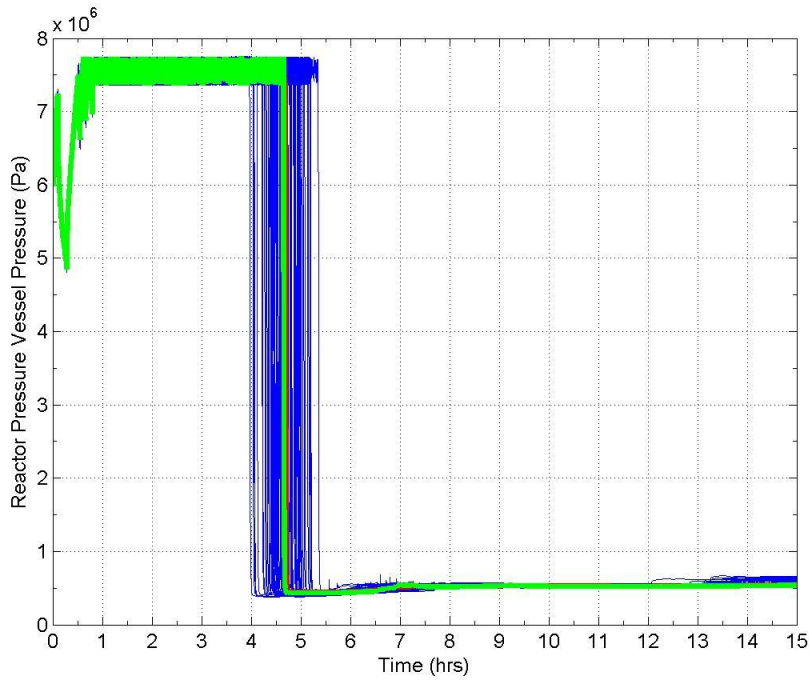
**Figure 4.1. Primary system pressure showing range of predicted main steam failure times.**

## 4.1.2 Core Water Level Boildown

The predicted reactor vessel water level for each realization is shown in Figure 4.2. From this figure we can see that predicted core uncovery times fall in a narrow band between about 2.2 and 2.4 hours. The water loss from the RPV during this time and up to about 4 hours is due to the periodic cycling of the SRV's and resulting venting of coolant inventory into the wetwell suppression pool. Based on emerging information from ongoing Fukushima analyses in the OECD BSAF program, it is further suspected that an additional RPV water loss not modeled in these analyses may have occurred from leaking recirculation pump seals, which if modeled, would advance the timing of core uncovering by some amount of time and accelerate other core degradation events. This unmodeled leakage of water inventory would result in a direct steam source to the drywell volume, bypassing the suppression pool and producing increased drywell temperatures and pressures during the first 5 to 8 hours of the accident. This previously unrecognized leakage of steam to the drywell will be included in future Fukushima sequence examinations.
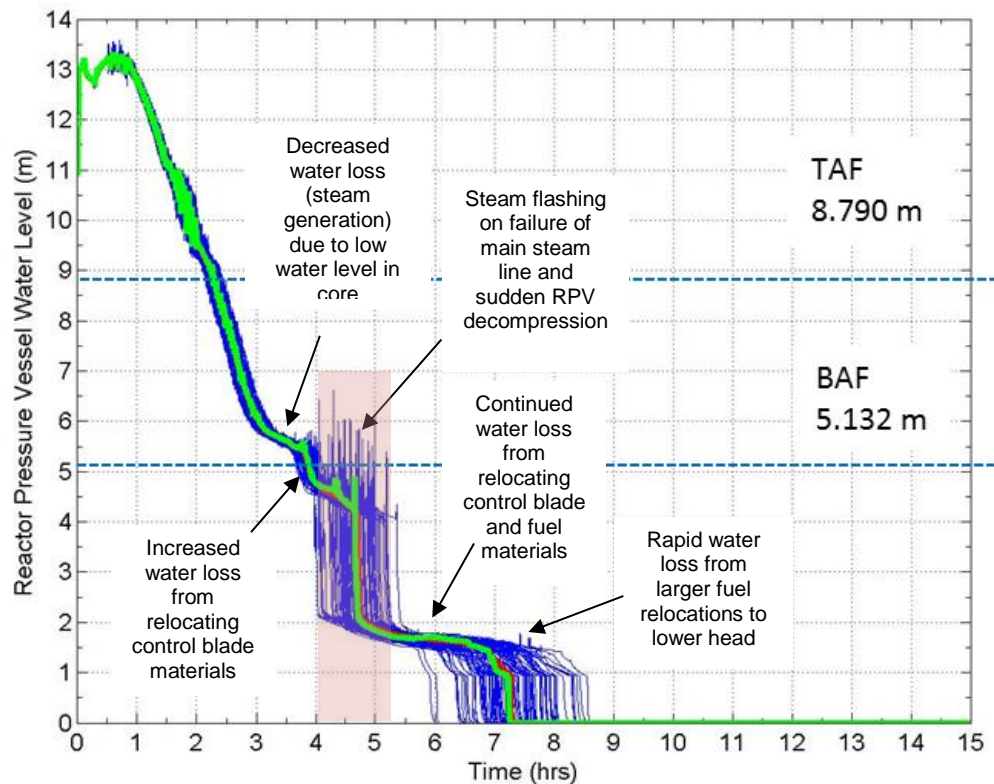
Reactor Pressure Vessel Water Level (m)

Decreased water loss (steam generation) due to low water level in core

Steam flashing on failure of main steam line and sudden RPV decompression

TAF
8.790 m

BAF
5.132 m

Continued water loss from relocating control blade and fuel materials

Increased water loss from relocating control blade materials

Rapid water loss from larger fuel relocations to lower head

Time (hrs)

**Figure 4.2. Reactor Vessel water level.**

The water level loss rate shows a decrease rate between 3 and 4 hours as the water level reaches the bottom of the core. This is due to decreased steam generation as less fuel "sees" liquid water and a greater fraction of decay heat is retained in the fuel rods caused by the gradual diminished steam cooling. Of course, as less heat is removed by steam cooling, more heat is retained in the fuel rods causing heatup, onset of Zr oxidation and hydrogen generation and the beginning of core degradation as the melting temperatures of the control blades and fuel rod cladding are progressively exceeded. Between 3.5 and 4 hours the core water level begins to sharply decrease due to the initial slumping of control blade materials and melted cladding Zr beginning to drop (drain) from the upper core to the lower core and core plate regions, quickly boiling down the residual water level in the core region.

During this time period core temperatures are rising rapidly, producing large amounts of hydrogen from Zr oxidation (discussed later) from the steam that is now being produced by the relocation of hot core materials into the lower core and lower plenum. This in turn produces high core exit gas temperatures that vent to the suppression pool through the cycling SRV. These hot gases flowing through the steam line of the cycling SRV are predicted to cause rupture of the steam line in the upper containment region and a sudden decompression of the RPV. Associated with this sudden drop in RPV pressure is the flashing of water in the RPV producing the sudden drop in water level in this time period as discussed earlier.

In the time frame between 4.5 and 6.5 hours, the RPV water level progressively decreases due to the boiling caused by the control blade and fuel materials that have gradually relocated to the

lower plenum. However, between about 6.5 hours and 8.5 hours a second large and sudden loss of water level is observed, this time due to the larger collapse and relocation of larger quantities of fuel components of the core into the lower plenum. The relocation of fuel bearing materials to the lower head causes the complete dryout of the lower head and starts the "clock" for lower head heatup and ultimate failure. Note however that lower head failure is not predicted for several more hours following head dryout as will become apparent from subsequent figures presented in this discussion.

### 4.1.3  Core Degradation and Relocation Events

The core relocation events that drive the RPV pressure response and loss of water from the RPV are described in the following discussions.  The two major phases of core relocation identified in the preceding, namely the initial relocation of lower melting point control blade materials followed later by the relocation of higher melting point fuel materials is shown in Figure 4.3 and Figure 4.4. These two major relocation events each cause significant steaming events as relocating materials come to rest in the lower core and lower plenum regions, and these steaming events in turn cause oxidation-driven temperature excursions and hydrogen generation. Note that between 6 and 8.5 hours, all remaining water in the lower head has been boiled away even as degrading core fuel bearing materials continue to accumulate in the lower plenum.

Close examination of Figure 4.3 and Figure 4.4 shows that the melting and relocation of control blade materials precedes the failure and relocation of the fuel materials, but that there is also an overlap of these processes for a period of time. (*Keep in mind that these results are statistical characterizations of the population and not a characterization of any particular realization*.) Eventually, the relocation of control blade materials from the core region to the lower plenum becomes essentially complete, while gradual relocation of fuel materials to the lower plenum persists for a longer period of time. Many realizations suggest that some residual fuel assemblies can remain intact. These remaining intact assemblies are found to be located on the periphery of the core where radial power profiles are low. This finding will be discussed later in the section on "Fukushima Decommissioning Insights." So a general observation is that initially low melting point control blade materials relocate downward, followed by a period of both control blade and fuel materials are relocating downward, and ending with a period where mainly fuel bearing materials drop to the lower plenum. This may result in a layering of material compositions initially accumulating on the lower head.

### 4.1.4  Hydrogen Generation

Hydrogen generation from the oxidation of Zr and stainless steel core components with steam is strongly dependent on temperature of the oxidizing materials and the availability of steam to support the reaction. Oxidation, hydrogen generation and rapidly escalating temperatures proceed concurrently until melting and relocation to lower cooler regions of the core takes place which has the effect of terminating hydrogen generation and peak temperatures locally. Hydrogen generation for the ensemble of realizations examined in this study is shown in Figure 4.5.

Hydrogen generation commences almost simultaneous with the first control blade relocations at about 3.5 hours, driven by sufficiently high temperatures (exceeding 1500K) and enhanced steam generation (control blade relocation to water in lower core and lower plenum). The two processes have an autocatalytic feedback effect – escalating temperature drives blade relocation, blade relocation drives steam generation, and steam generation drives oxidation and temperature escalation and increased blade relocation.

The escalating temperatures driven by the oxidation transient, fortified by increased steaming from blade relocation, produces high gas temperatures flowing through the steam line of the lowest pressure setpoint SRV, as discussed earlier, and this in turn precipitates rupture of the steam line due to high temperature and high pressure. The sudden depressurization flashes the RPV water to steam, which temporarily cools the core region and ultimately reduces steam production as the water level falls well below BAF. The result of this event is to temporarily suppress hydrogen generation as seen in Figure 4.5 in the time range between 4 and 5.5 hours.

Hydrogen generation resumes however between 5.5 hours and 8 hours as fuel bearing materials relocate to the water-filled lower plenum (Figure 4.4) when steam generation invigorates oxidation of hot Zr-components still resident in the core region. Eventually, as core materials continue to relocate to the lower plenum and the water inventory in the RPV is depleted, the hydrogen generation again levels off. The range of maximum hydrogen generation at the end of this sequence of events is predicted to be between about 675 and 900 kg.
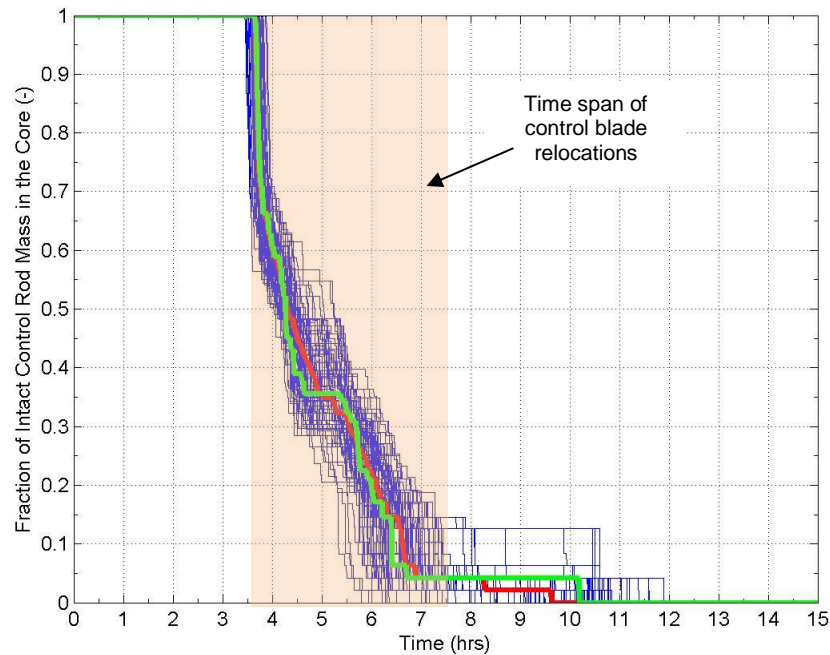


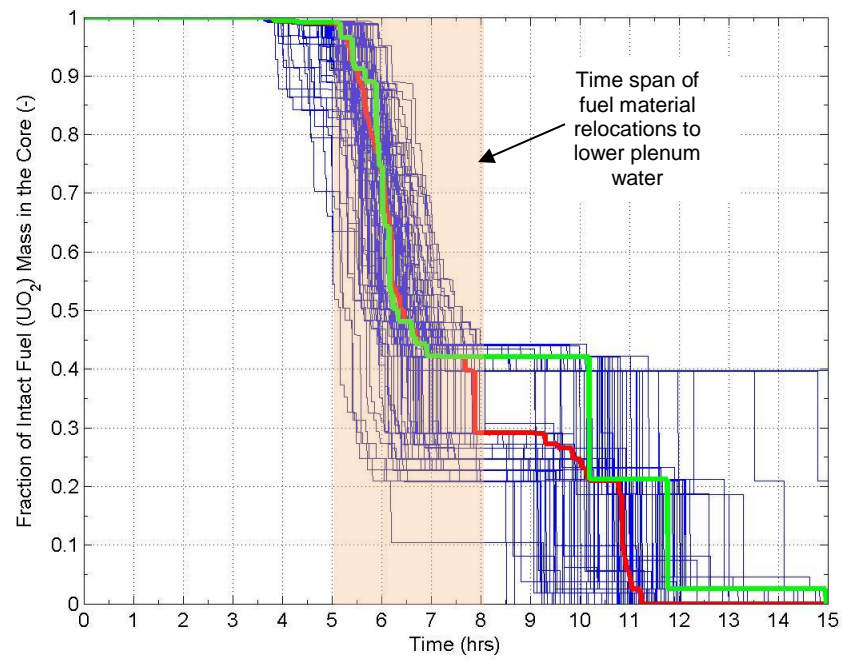**Figure 4.3.  Fraction of intact control rod mass in the core.**

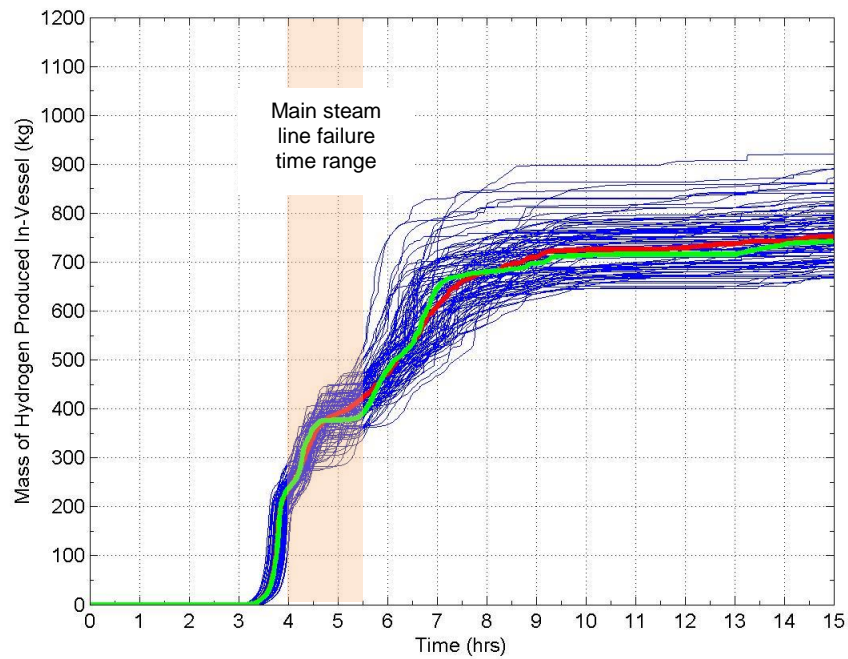**Figure 4.4.  Fraction of intact fuel mass in the core.**



**Figure 4.5.  Mass of hydrogen produced in-vessel.**

28

### 4.1.5  Lower Head Failure and Core Material Relocation to Reactor Cavity

As seen in Figure 4.2 the reactor lower head water dryout is predicted to take place between 6.5 and 8.5 hours, after which steady heatup of the lower core debris accumulations transfer heat to the RPV lower head. More than half of the realizations did not predict lower head failure by 15 hours when emergency cooling water was injected by core spray line. Had cooling water not been injected, these cases would have eventually led to head failure. For those cases that did result in lower head failure, it was from loss of strength as the inner vessel wall material melts under the heat load from the core debris. The predicted mass released to the cavity region is shown in Figure 4.6. For the most part, on failure of the RPV lower head, most accumulated materials are released to the reactor cavity within 10 or 15 minutes; however in some realizations the transfer of materials proceeds over a protracted period, perhaps an hour or so. Most realizations relocate a large fraction of the total core inventory, suggesting a generally large degree of core failure and ultimate transfer to the cavity region. However, as discussed earlier, some fraction of realizations suggest that not all regions of the core are failed and that some residual core materials can be expected in the peripheral regions of the core. This will be discussed further in the following section on decommissioning implications.
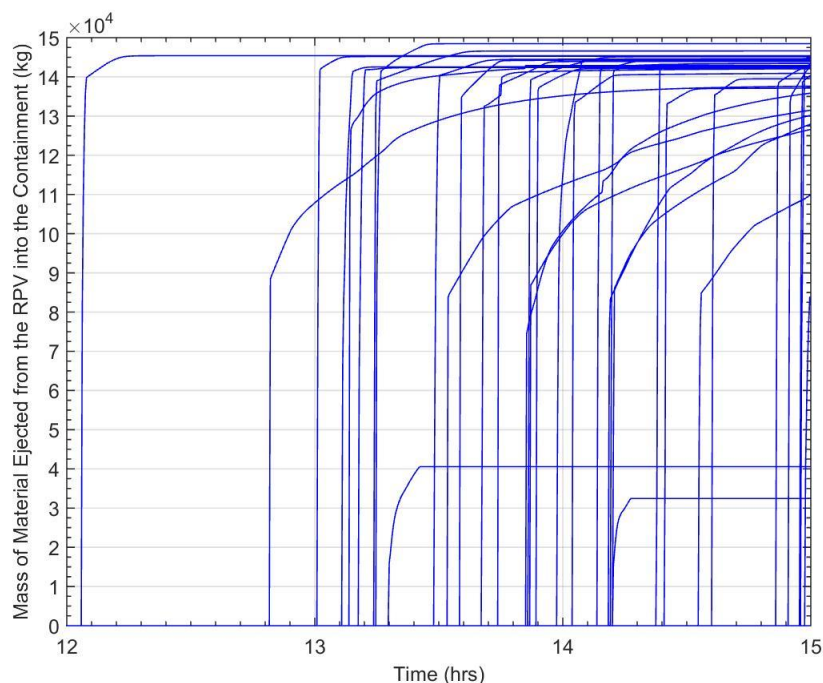


**Figure 4.6.  Mass of core material ejected to the reactor cavity.**

### 4.1.6  Containment Pressure Response

The containment drywell and wetwell pressures, shown in Figure 4.7 and Figure 4.8 respectively show the response to the SRV venting steam to the suppression pool as well as the RPV depressurization event. The SRV venting period prior to the main steam line rupture brings about a gradual increase in wetwell/drywell pressure as the water in the suppression pool increases in temperature gradually increasing the saturation pressure of the wetwell and the entire containment. This gradual increase in drywell and wetwell pressure during the SRV cycling

period appears to produce correspondingly higher containment peak pressures at the timing of main steam line rupture, presumably due to diminished heat sink available in the wetwell at the actual time of RPV blowdown. Subsequent to the MSL rupture time, containment pressures gradually increase in time owing to increased accumulation of decay heat in the containment (recall the containments are isolated from the ultimate heat sing of the ocean). Sporadic sharp increases in containment pressure are driven by melt relocation events from the core to the lower plenum of the vessel during the time frame of 5.5 to 7.5 hours, where intense steam generation in the lower plenum translates to corresponding increases in containment pressure.

The late-time "step" increases in containment pressures in the 12 to 15 hour time period are associated with lower head failure when core debris falls to the reactor cavity floor producing additional steam generation from debris contact with water present in the cavity region from the earlier MSL rupture, and a corresponding containment pressure response.

The DW and WW pressures tend to track each other over the duration of the simulation, as they must since they are closely coupled aside from a small hydrostatic head difference associated with the submergence of the drywell vents below the water level in the wetwell suppression pool. As discussed earlier, significant increases in both the DW and WW pressures begin coincident with the start of fuel failure; this is due to material relocation into the remaining water in the core, resulting in the production of steam.
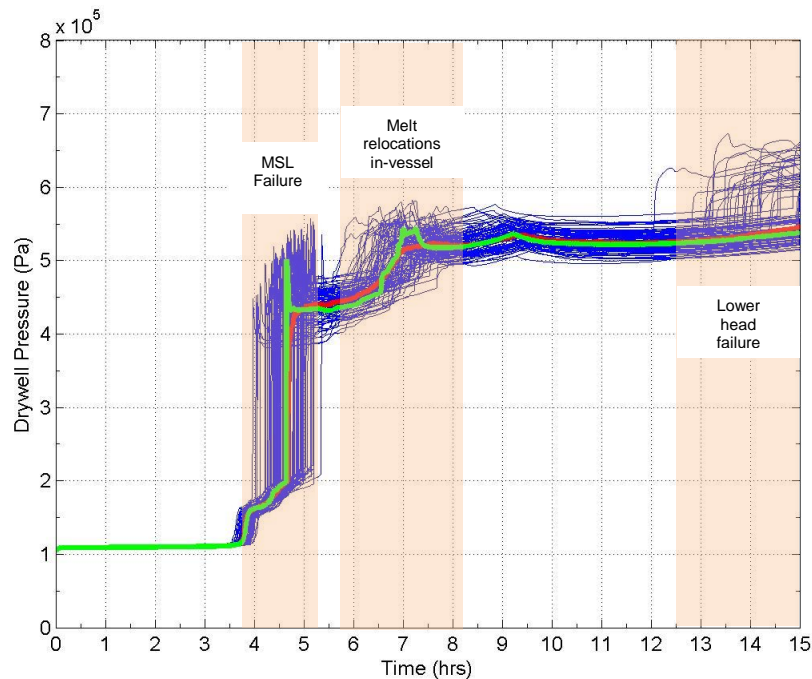


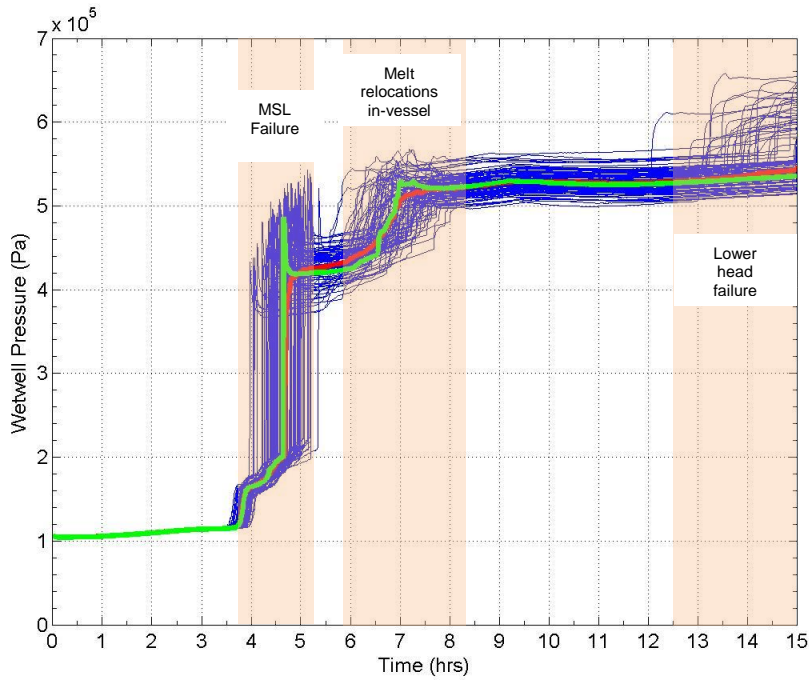**Figure 4.7. Containment drywell pressure response.**

**Figure 4.8.  Containment wetwell pressure response**

## 4.2    Observations and Areas of Future Improvement

Direct comparisons to Fukushima data have not been made in this study, and while the prediction of these analyses are generally consistent with the available accident response data, some differences remain where we have good insights into future improvements in these analyses. Examples include the modeling of a direct steam leakage to the drywell from leaking recirculation pump seals, and recognition of the need to increase in drywell containment nodalization (to capture local heating caused by MSL rupture), both aimed at improving our comparison to measured containment pressure response. The timing of core damage events is generally consistent with known accident progression trends. In this study, lower head failure is judged to be a bit too late compared to Fukushima data trends, mainly the drywell pressure response and radiation detection at the Fukushima main gate, which strongly suggest lower head failure at around 12 hours in comparison to the 13 to 15 hour range inferred by these analyses – in fact most realizations (about 2/3's) did not result in lower head failure by 15 hours. Improvement in these accident signatures is expected base on new and emerging understanding of these accidents. However, the general trends concerning degree of damage to core region, retention of core materials in the RPV, and the ultimate mass of materials transferred to the reactor cavity region are considered reasonable and informative for planning of decommissioning activities.

The following section addresses specific decommissioning issues that can be informed by these uncertainty analyses.

# 5      IMPLICATIONS FOR FUKUSHIMA DECOMMISSIONING

The Nuclear Damage Compensation and Decommissioning Facilitation Corporation (NDF) has been established in Japan in part to facilitate and coordinate development of decommissioning technologies that will be needed in order to defuel and decommission the damaged reactors at the Fukushima Daiichi Nuclear Power Station. NDF has sought insights from severe accident code analyses performed under the OECD-NEA BSAF[6] project. The selected figures of merit examined in this uncertainty study were aimed at providing such key insights to the decommissioning activities. In order to design defueling equipment and strategies it will be most helpful to understand the degree of damage in the reactor cores, the expected final distribution of core materials within the original core region, fuel debris remaining in the vessel lower head region and expected amounts of material that exited the reactor pressure vessel and fallen to the reactor pedestal/cavity floor.

This uncertainty study explores those damage characteristics and presents potential ranges or distributions for those characteristics to inform the decommissioning activities about the range and likelihood of expected damage configurations and thereby provide the information useful to specifying design requirements for decommissioning equipment and strategies. The figures of merit explored in this study are the principal obvious quantities of first order importance in decommissioning actions; however, future analyses could be performed to inform the expected conditions in the Units 2 and 3 Fukushima Daiichi reactors and additional figures of merit defined to address more specific questions and issues as decommissioning activities move forward. Uncertainty analyses provide a far broader spectrum of information than is possible from single deterministic analyses. The following sections review those key figures of merit and provide additional interpretation on decommissioning implications.

## 5.1    Relocation of Control Blades and Fuel Bearing Materials to Lower Vessel Head

Because of the lower effective melting temperature of the stainless steel/$B_4C$ control blades (about 1500K owing to boron-iron eutectic formation), the control blade components are the first major core components to melt and drain from the core region. Figure 4.3 showed the "horsetail plot" results for all uncertainty realizations as a function of time. In a sense, the horsetails plots provide graphical visualization of the time-varying probability density function. The uncertainty information may be presented in a slightly different manner by forming approximations for the cumulative distribution function at selected times by arranging the values at any point in time in rank order and plotting the cumulative fraction of the values that are less than the specified ordinate value. The control blade fraction remaining in the core is shown in this way in Figure 5.1 for times of 4.8, 5.8, 10 and 15 hours. (*These selected times are somewhat arbitrary but were chosen to coincide with observed events in the control blade and fuel material failures.*) From this figure we can see that at 4.8 hours essentially all realizations exhibited no more than about 58% of control blade material remaining in the core region and no realizations exhibited less than about 27% of blade material. Put another way, all cases by 4.8 hours had relocated between

---

40% and 73% of the control blade materials to the core plate or lower plenum. By 5.8 hours, all cases relocated at least 60% of control blade materials to the lower core or lower plenum region and about 10% of the cases had relocated between 80 and 100 percent of control blade material to lower core plate or below. By 10 hours, 60% of cases have relocated all control materials to lower core plate or below, about 35% have relocated 95% of control blade material and only about 5% of cases have relocated less than 90% of control blade materials. By 15 hours, all realizations have relocated all in-core control materials to the lower core plate and below.
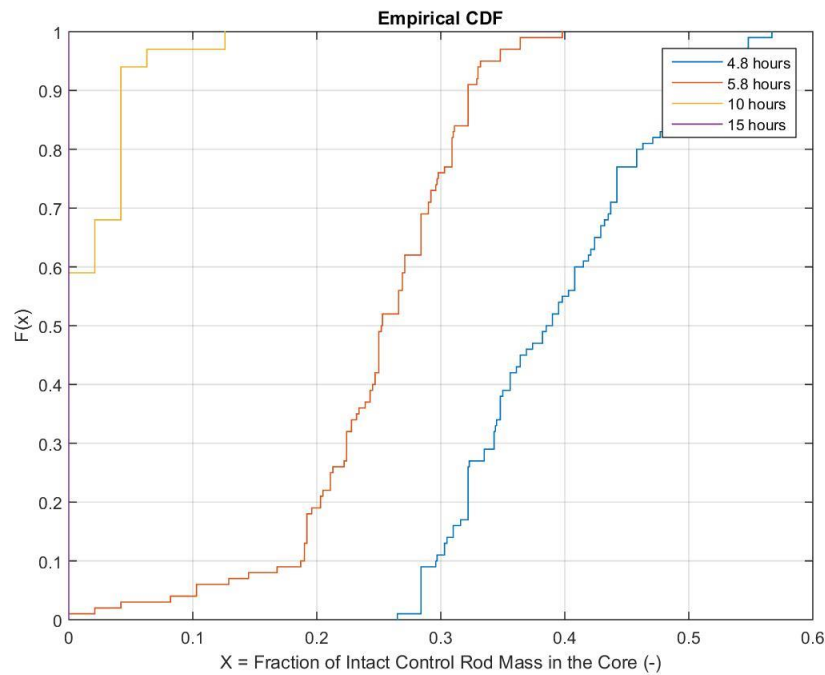


**Figure 5.1.  Fraction of Intact Control Blade Mass in Core Region.**

The undamaged fuel materials remaining in the core region shown in Figure 5.2 follows a similar trend except lagging in time behind the control blade relocations and some cases suggest a residual amount on undamaged fuel remaining in the core region by 15 hours. By the end of the core damage phase, about 2 percent of the cases show up to 30% of the fuel remaining in the core while 8 % or the realizations predicted a few percent of the fuel assemblies to be remaining undamaged in the core region.

Ignoring spatial incoherencies across the core, these trends suggest a layering of materials may have accumulated in the lower reactor head, where early in time, this lower-most layer is comprised of mainly control blade materials (from 50% to 70% of the total amount of control blade materials), namely stainless steel and boron carbide with very little fuel bearing materials. For a while both control blade materials and fuel bearing materials are relocating downward at the same time, but perhaps not coherently from a spatial point of view. These accumulations may be comprised of comparable fractions of core totals of control blade and fuel bearing materials. And towards the end of the core slumping period, mostly fuel bearing materials are relocating downward on top of the previously accumulated debris.
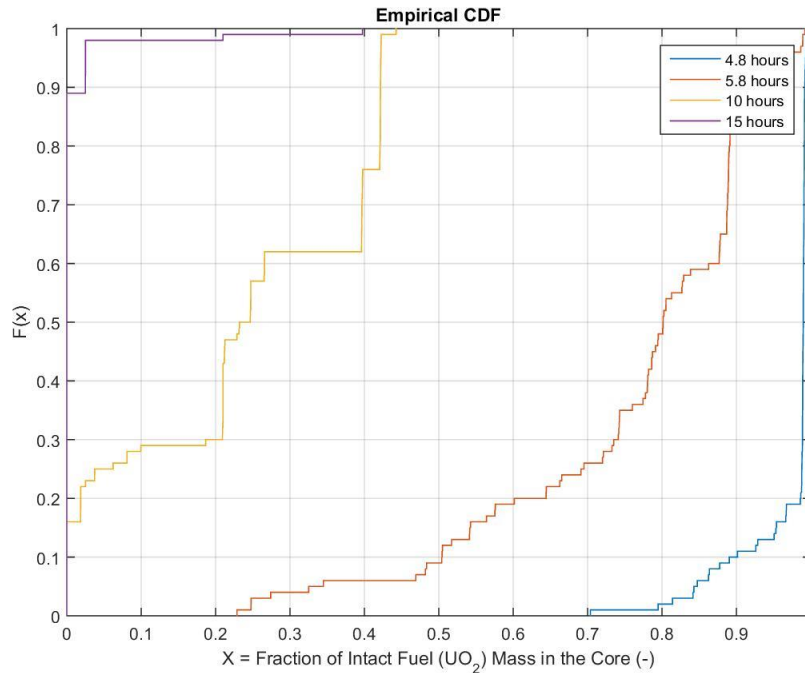
**Figure 5.2. Fraction of Intact Fuel Mass in Core Region.**

## 5.2 Relocation of Lower Head Materials into Reactor Cavity

Shown in Figure 5.3 is the CDF for the mass of core materials ejected to the cavity following failure of the vessel lower head. Note that in this case not all realizations actually resulted in lower head failure by 15 hours, the time at which water injection was restored to the Unit 1 reactor. This reveals both a bias in the MELCOR predicted head failure time, as the Fukushima Daiichi Unit 2 vessel head is widely thought to have failed at about 12 hours, whereas the central tendency of the realizations for this study was centered more in the 13 to 15 hour time frame. Causes for this apparent bias will be investigated further in future studies, but the finding also suggests that the Unit 1 reactor damage progression perhaps had some chance of being arrested had the water injection been accomplished a few hours sooner.

The CDF shown in Figure 5.3 was formed conditional on the lower head having failed before the 15 hour time of water injection. The realizations shown in the horsetail plots of Figure 4.6 and the conditional CDF in Figure 5.3, reveal that in most cases head failure results in the rapid discharge of most of the accumulated debris of the lower vessel. About 60% of the realizations with lower head failure resulted in the discharge of 95 to 100% of the core material accumulated in the lower head. About 30% of the cases ejected between 80 to 95%, while about 5% of the cases showed ejection of only about 30% of the lower head debris accumulations.
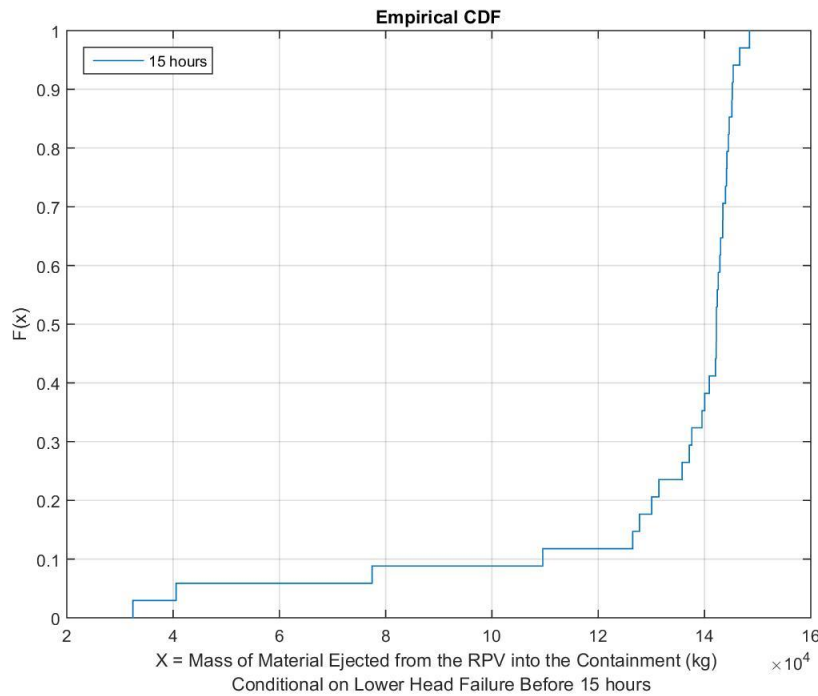
35

**Figure 5.3.  Mass of Core Materials Ejected to Reactor Cavity.**


## 5.3   Conclusions of Material Relocation Analysis

These results suggest that most fuel bearing and control blade materials are expected to have relocated from the core region to the lower vessel head and that a layering of accumulations might have been formed by the relocations with the lower-most layer comprised of about half of the control blade stainless steel and boron carbide. Subsequent layers of debris with mixtures of fuel bearing debris and control blade material are suggested with the final core material falling to the lower head being largely comprised of fuel bearing materials. Not investigate in this study is the ultimate fate of the significant lower plenum stainless steel control rod guide tubes which would have been subsumed into this layered accumulation of core materials. This possibility could be further investigated in a future study. In that compounds that include boron carbide can be among the hardest materials known to exist, some of these aggregations implied in these observations could prove quite challenging to the defueling process. This study implies that the decommissioning activities can expect to encounter some residual fuel assemblies remaining in the core regions, likely on the periphery of the core, perhaps 15 to 20% of the lower head debris accumulations retained in the head regions (or on the drive tubes that reside below the vessel head – not currently modeled in MELCOR), and as much as 80 to 100 % of the core materials relocated to the cavity region. Because of the layering suggested by the time-phased relocation of control blade and fuel bearing materials, the debris accumulations may not be homogeneous in nature, something to bear in mind when designing defueling equipment.

## 5.4 Hydrogen Generation

For completeness, cumulative distribution functions were estimated from the hydrogen horsetail results and are shown in Figure 5.4. The spread in the predicted hydrogen generation shows a similar dispersion around the median values for the 4 time periods selected. As time progresses, the total amount of hydrogen steadily increases and the upper end of the hydrogen predicted at 5.8 hours shows a greater dispersion than the lower end of the CDF. By 10 hours, most of the hydrogen that could be produced has been realized and only a little more hydrogen is seem by the end of the sequence analyses at 15 hours. This is both due to consumption of available metallic zirconium by oxidation, its relocation to cooler regions of the reactor vessel, as well as by the termination of steam generation from boildown and water loss. Such characterization of hydrogen generation can facilitate design and placement of hydrogen igniters and recombiners by providing information on the maximum quantities that can be realized and the timing of hydrogen generation. While informative on hydrogen generation and its uncertainty, these results do not bear strongly on decommissioning issues other than to indicate the possible maximum quantities of oxidized cladding and channel box materials that will be encountered in the defueling activities.
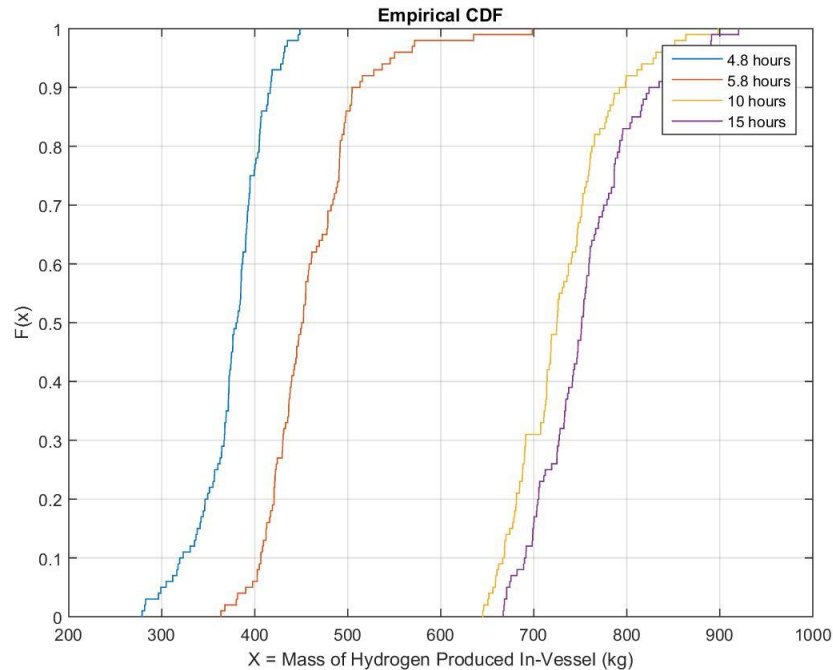


**Figure 5.4. Hydrogen Generation Results shown in CDF format.**

# 6    A QUANTIFICATION OF CODE NUMERICAL SENSITIVITY WITH IMLICATIONS ON PRECISION OF COMPUTED RESULTS

In order to assess MELCOR sensitivity to the parameters varied in this uncertainty study and to quantify known code numerical inherent noise levels in response to response to changes in code input values, a special case was examined where the same uncertainty parameters were considered except that their sampled distributions were narrowed considerably such that only small changes in each sampled parameter around a central value were sampled. A mean-like member of the main study (realization number 13) was used so that the central tendency of the narrow distribution sensitivity study should closely resemble the central tendency of the main uncertainty study. The narrowed distribution parameters are summarized in Table 6.1 where about 1% variation around the central value was allowed in the sampling process.

The results of the small perturbation variations are shown to the right of the base case results of the uncertainty distribution in Figure 6.1 through Figure 6.8 to highlight the degree of numerical noise that results from small changes in code input values. Some general observations can be made from these comparisons. Firstly, the central values of the small perturbation realizations are largely consistent with the central tendencies of the full uncertainty study results. This suggests that code accuracy is maintained while varying the inputs over a small range.[7] The small perturbation results however show the inherent limitations on code precision where some degree of scatter in results about a central tendency remains as parameter range variations are reduced to small values. Secondly, the variation in results from the full uncertainty analysis covers a larger span than does the small perturbation analyses. This implies that we can tell the difference between true uncertainty variance and the underlying numerical variations even though the residual numerical variation is on the same order of magnitude as our uncertainty results. Thus these results both qualitatively quantify our predicted uncertainty ranges due to state of knowledge uncertainty as well as our code model precision level.

Examination of Figure 6.4 and Figure 6.5 suggest that material relocations events may be important contributors to the scatter in subsequent code results possibly due to the large impacts on the solution matrix as sudden large movements of core materials take place. This will be a subject of further investigation in future studies.

---

[7] Here accuracy implies that the central tendency of the code scatter in results is maintained. That is to say that the code produces consistent results on average for the given input values. Precision on the other hand is used to describe the size of the scatter around the central tendency.

**Table 6.1 – Small Change Distributions Based on Rlz13 Sampled Values.**

| parameter | nomenclature | uniform distribution |
|---|---|---|
| time constants for radial (solid) debris relocation | SC1020_1 | L.B. = 4.3004E+02<br>Rlz13 = 4.3220E+02<br>U.B. = 4.3436E+02 |
| time constants for radial (liquid) debris relocation | SC1020_2 | L.B. = 6.5580E+01<br>Rlz13 = 6.5910E+01<br>6.6240E+01 |
| dT/dz model, time constant for averaging flows | SC1030_2 | L.B. = 9.1232E-02<br>Rlz13 = 9.1690E-02<br>U.B. = 9.2148E-02 |
| dT/dz model, characteristic time for coupling dT/dz temperatures to average CVH volume temperature when dT/dz model is active | SC1030_4 | L.B. = 8.8286E+00<br>Rlz13 = 8.8730E+00<br>U.B. = 8.9174E+00 |
| dT/dz model, maximum relative weight of old flow in smoothing algorithm involving time constant for averaging flows | SC1030_5 | L.B. = 5.6377E-01<br>Rlz13 = 5.6660E-01<br>U.B. = 5.6943E-01 |
| molten zircaloy melt break-through temperature | SC1131_2 | L.B. = 2.3492E+03<br>Rlz13 = 2.3610E+03<br>U.B. = 2.3728E+03 |
| molten cladding (pool) drainage rate | SC1141_2 | L.B. = 3.4367E-01<br>Rlz13 = 3.4540E-01<br>U.B. = 3.4713E-01 |
| fraction of strain at which lower head failure occurs | SC1601_4 | L.B. = 1.7313E-01<br>Rlz13 = 1.7400E-01<br>U.B. = 1.7487E-01 |
| scaling factor for candling heat transfer coefficients | cor_cht_hfzrXX | L.B. = 1.0826E+00<br>Rlz13 = 1.0880E+00<br>U.B. = 1.0934E+00 |
| fraction of un-oxidized cladding thickness at which thermal-mechanical weakening of oxidized cladding begins | cor_rod_2 | L.B. = 1.3094E-03<br>Rlz13 = 1.3160E-03<br>U.B. = 1.3226E-03 |
| debris quenching heat transfer coefficient to pool | cor_lp_2 | L.B. = 9.8654E+02<br>Rlz13 = 9.9150E+02<br>U.B. = 9.9646E+02 |
| debris falling velocity | cor_lp_4 | L.B. = 4.6894E-01<br>Rlz13 = 4.7130E-01<br>U.B. = 4.7366E-01 |
| minimum debris porosity (Lipinski dryout model); SC1244(1)<br>min. porosity used in flow blockage Ergun pressure drop equation; SC4413(5)<br>min. hydrodynamic volume fraction; SC4414(1)<br>minimum porosity to be used in calculating the flow resistance in the flow blockage model; SC1505(1)<br>minimum porosity to be used in calculating the area for heat transfer to fluid; SC1505(2) | minpordp | L.B. = 8.9968E-02<br>Rlz13 = 9.0420E-02<br>U.B. = 9.0872E-02 |
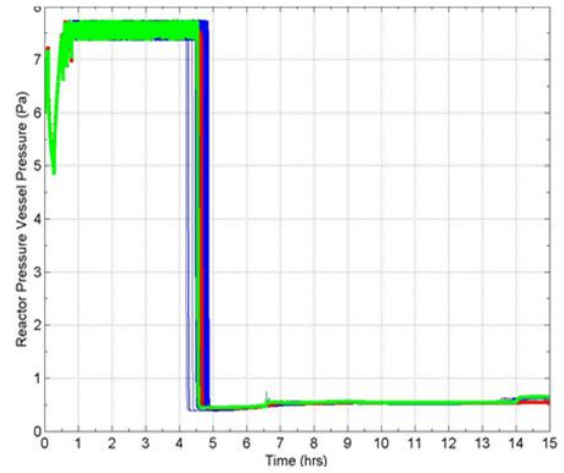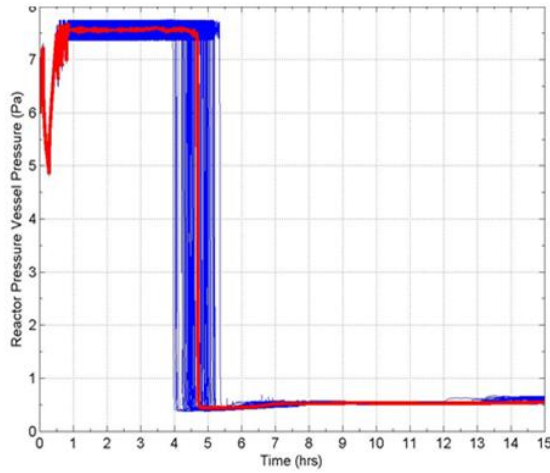
**Figure 6.1.  Base Case Comparison with Small Perturbation analysis (RPV pressure).**
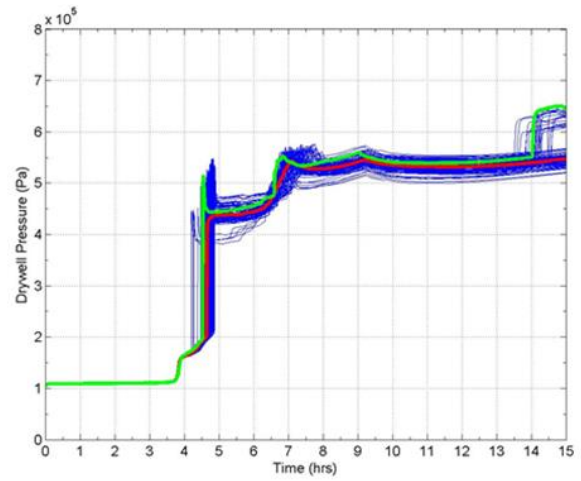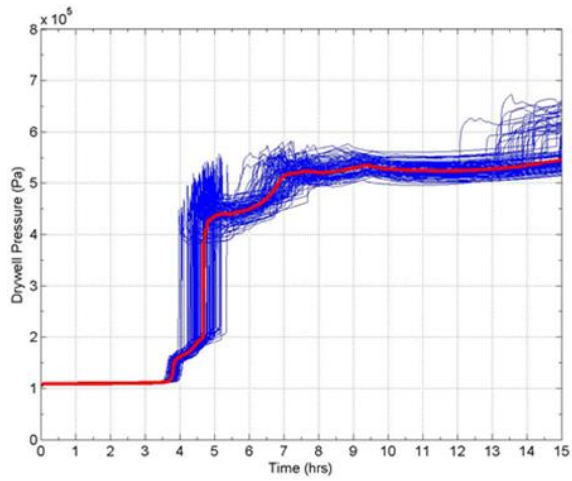


**Figure 6.2.  Base Case Comparison with Small perturbation analysis (Drywell Pressure).**
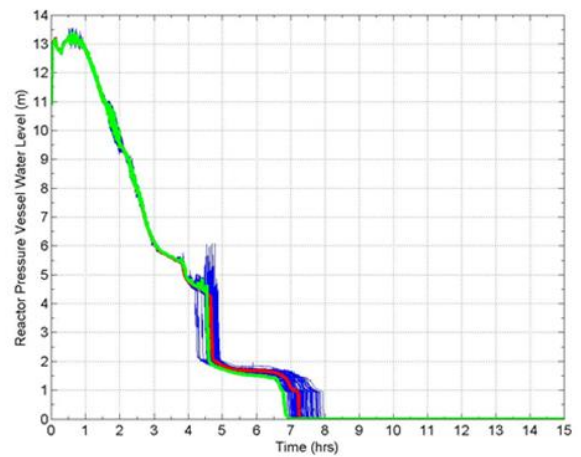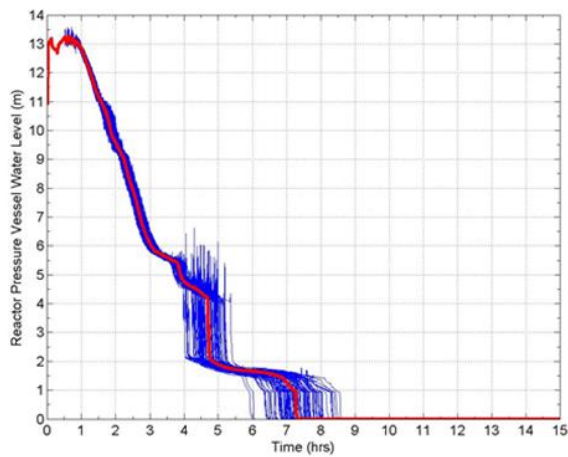


**Figure 6.3.  Base Case Comparison with Small Perturbation analysis (RPV Water Level).**
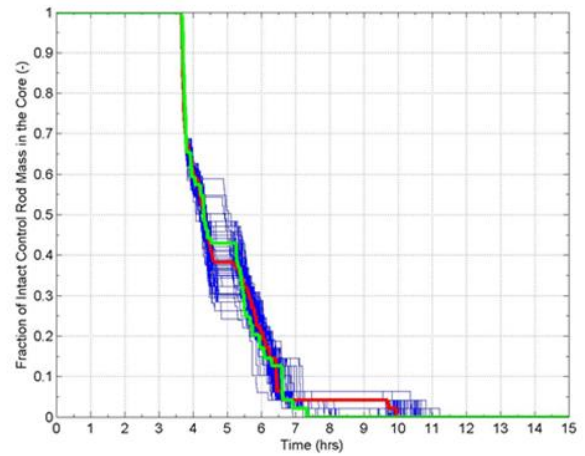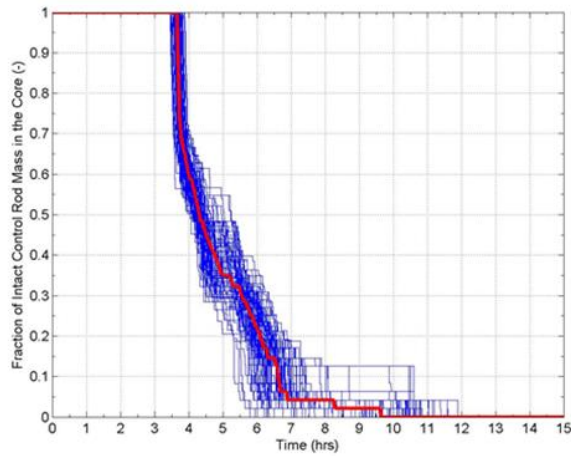
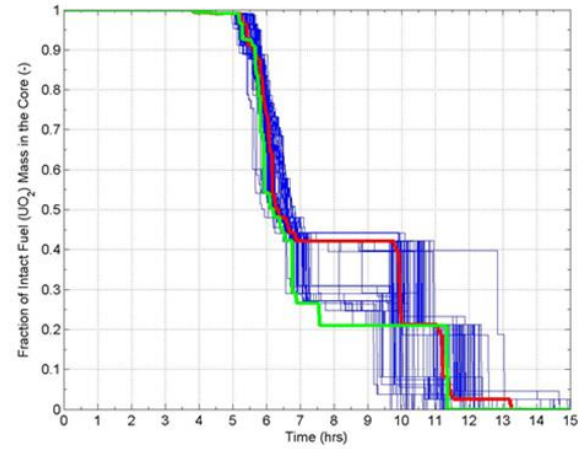**Figure 6.4.  Base Case Comparison with Small perturbation analysis  Intact Control Rod Mass).**
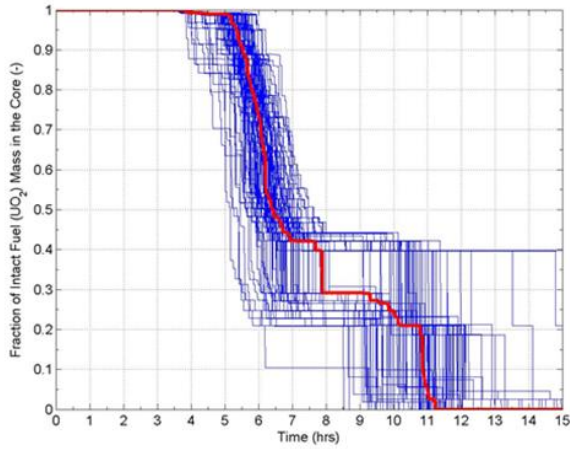


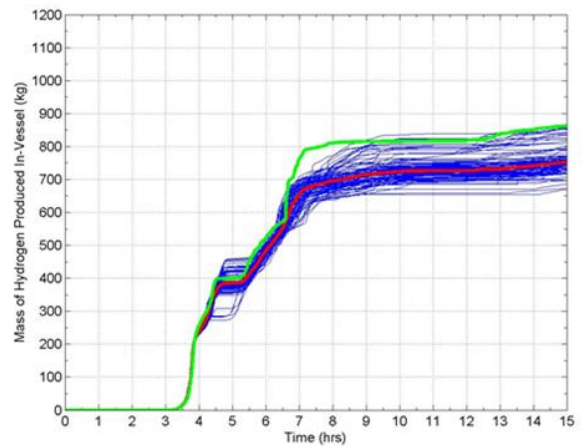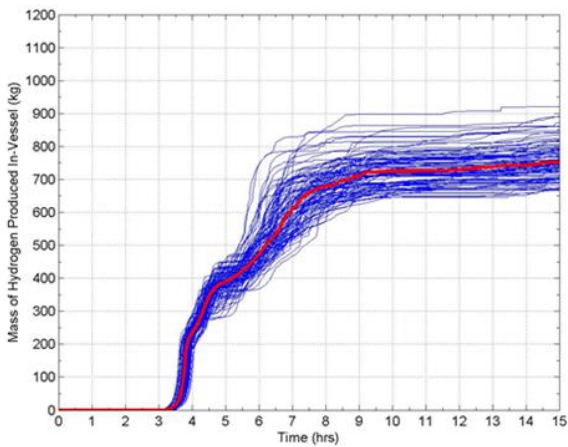**Figure 6.5.  Base Case Comparison with Small perturbation analysis Intact Fuel Mass).**



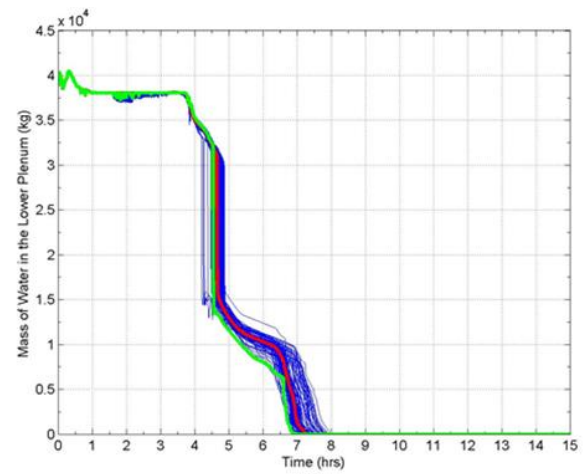**Figure 6.6.  Base Case Comparison with Small perturbation analysis (In-Vessel Hydrogen).**
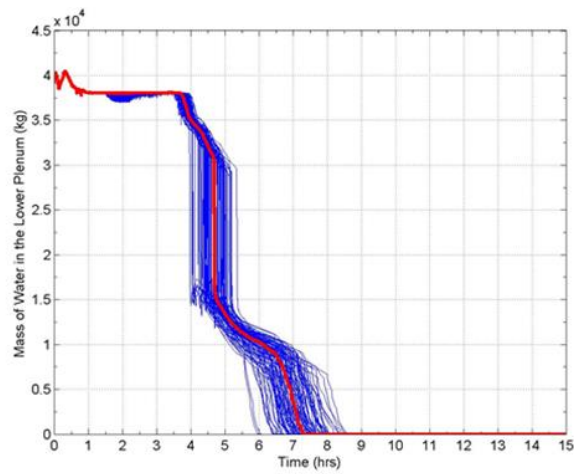
**Figure 6.7. Base Case Comparison with Small perturbation analysis (Mass of Water in the Lower Plenum).**
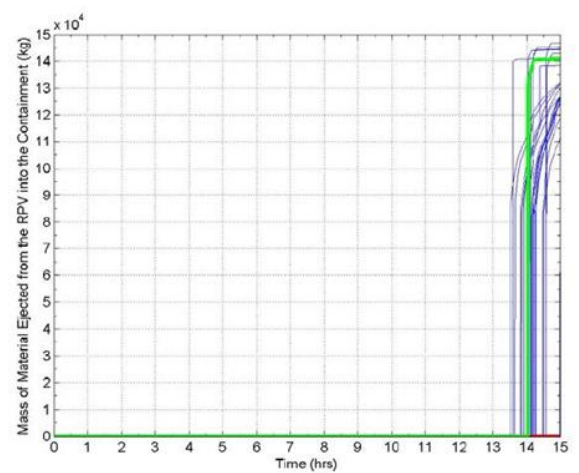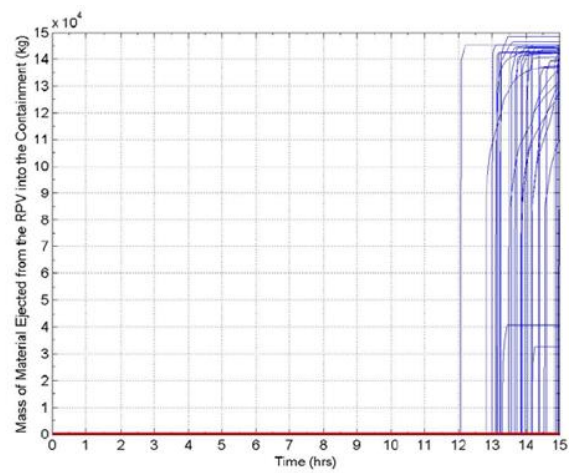


**Figure 6.8. Base Case Comparison with Small perturbation analysis (Mass of Material Ejected).**

# 7    SUMMARY AND CONCLUSIONS

An uncertainty analysis was performed for the Fukushima Daiichi Unit-1 accident sequence focused primarily on melt progression uncertainties as modeled in MELCOR. MELCOR input parameters known to affect melt progression behavior were treated as uncertain where distributions of parameter values were estimated to reflect the state of knowledge uncertainty for these key code parameters. The parameters were sampled randomly to produce 100 MELCOR realizations (predictions) reflecting this uncertainty in the range of their predicted variations. A primary motivation for this study was to identify ranges of predicted core damage states in order to inform future decommissioning activities for the damaged reactors at the Fukushima site. Key figures of merit were identified as code output aimed at characterizing potential reactor damage states such as state of damage to core control blades, fuel rods in the core, and their relocation and redistribution throughout the core region, lower vessel region and reactor pedestal/cavity region for cases where lower head failure was predicted within the first 15 hours of the accident. Hydrogen generation during the core damage progression was also investigated.

From these results several key findings were observed. One of these findings is that the control blade failure and relocation initiates prior to the first fuel damage events and results in the stainless steel and boron carbide blade materials draining downward to the lower core plate and vessel lower plenum. About half of the control blade materials have relocated downward before the first fuel rod failures occur. Then for a while, both control blade and fuel rod failures occur simultaneously, mainly due to temporal and spatial incoherencies across the core. Finally, there is a period where only fuel rod failures produce downward relocation events. We suggest that this could produce a layering of materials with lower melting point control blades are rich in the lower accumulations in the vessel lower head, with mixtures of control blade and fuel material, followed last by an upper layer of fuel rich accumulations.

The results also suggest that some relatively undamaged fuel assemblies could still be in the core regions around the periphery of the core and that some residual debris of control blade and fuel material may also have been retained in the vessel lower head. Most cases that predicted lower head failure before 15 hours suggested a rapid and nearly complete relocation to the reactor cavity region (recalling that some cases showed residual material retained in the vessel lower head). These general findings can inform anticipated Fukushima decommissioning activities by identifying the regions both in-vessel and ex-vessel where fuel materials are likely to be found.

Not addressed in this study are potentially significant implications concerning high temperature damage to the vessel upper internal components, chiefly steam separators and dryers. Damage to these components from high core exit gas temperatures could significantly complicate their removal in the decommissioning phase. Future studies could address logistical issues such as this.

The study was scoping in nature and several areas of potential improvement were identified to improve accident signatures such as better prediction of lower head failure timing and improved comparison to containment pressure data. Such refinements will improve the accuracy of the predicted figures of merit and provide better guidance to decommissioning activities.

Characterizing the effect of uncertainty on the anticipated core and vessel damage states helps ensure that a more complete range of potential damage states are identified.

Results presented in this study considers effects of the codes numerical precision through a comparison of sampled results from narrow-range uncertainty input uncertainty distributions. This was done to quantify the order of magnitude of the numerical precision that can be expected of complex multi-effects codes, in this case MELCOR, in the midst of broader state of knowledge variations employed in the uncertainty analysis. It was shown that this presently irreducible variability is smaller than the variation of results produced from sampling the full range of uncertain inputs, although of the same order of magnitude. It was also shown in the reduced range sampling study that the central tendency of the sampled results was not shifted from the full uncertainty range sampling results. This means that the numerical imprecision, while adding to the complexity of quantifying the sensitivity of the uncertainty in the input to the variability in the output, must be considered when assessing the magnitude of variance in the results.

The utility of this methodology in identifying a broad range of plausible damage states for assisting in decommissioning planning has been demonstrated and areas of improvement identified. The methodology could be readily extended to the other Fukushima Daiichi Unit 2 and Unit 3 accident sequences and thereby similarly inform decommissioning activities for these reactors as well.

# 8 REFERENCES

1.    R.O. Gauntt, et al., NUREG/CR-6119, "MELCOR Computer Code Manuals, Vol. 2: Reference Manuals, Version 1.8.6 (Vol. 2, Rev. 3)," Sandia National Laboratories, Albuquerque, NM, 2005.

2.    R.O. Gauntt, et al., SAND2012-6173, "Fukushima Daiichi Accident Study (Status as of April 2012)," SNL, Albuquerque, NM, 2012

3.    U.S. Nuclear Regulatory Commission, State-of-the-Art Reactor Consequence Analyses (SOARCA) Report, NUREG-1935,Washington, DC, 2012.

4.    Sandia National Laboratories, NUREG/CR-7155, "State-of-the-Art Reactor Consequence Analyses Project: Uncertainty Analysis of the Unmitigated Long-Term Station Blackout of the Peach Bottom Atomic Power Station – DRAFT Report," USNRC, Washington, DC, 2013. 2012.

5.    State-of-the-Art Reactor Consequence Analyses Project Uncertainty Analysis of the Unmitigated Short-Term Station Blackout of the Surry Power Station" DRAFT Report.

6.    M. Pellegrini, "Benchmark Study of the Accident at the Fukushima Daiichi Nuclear Power Plant, Phase I Report", The Institute of Applied Energy, Nuclear Power Engineering Center, Tokyo, Japan. 2015.

7.    D. Luxat, D. Kalinich, J. Hanophy, 3002004449, "Modular Accident Analysis Program (MAAP) – MELCOR Crosswalk, Phase 1 Study," EPRI, Palo Alto, CA, 2014.

8.    U.S. NRC. "State-of-the-Art Reactor Consequence Analysis Project, Volume 1: Peach Bottom Integrated Analysis," NUREG/CR-7110, Volume 1, U.S. Nuclear Regulatory Commission: Washington DC. 2012.

9.    M.T. Leonard, R.C. Nause, R.O. Gauntt. "A General Purpose MELCOR Model of a BWR/4 Mark I Nuclear Power Plant," DRAFT, Sandia National Laboratories, Albuquerque, NM. 2008.

10.   Distribution of 1F1-3 plant specifications". Letter and enclosures from F. Nagase (JAEA) to R.O. Gauntt (SNL), October 13, 2013.

11.   J.J. Carbajo. "Severe Accident Source Term Characteristics for Selected Peach Bottom Sequences Predicted by the MELCOR Code." NUREG/CR-5942, Oak Ridge National Laboratory: Oak Ridge, TN. July 1993.

12.   D.A. Powers, et al. "Accident Source Terms for Light-Water Nuclear Power Plants Using High-Burnup or MOX Fuel," SAND2011-0128, Sandia National Laboratories: Albuquerque, NM. January 2011.

13.   L. Soffer, et al. "Accident Source Terms for Light-Water Nuclear Power Plants," NUREG-1465, U.S. Nuclear Regulatory Commission: Washington, DC. February, 1995.

14.   K. Ross, et al., "MELCOR Best Practices as Applied in the State-of-the-Art Reactor Consequence Analyses (SOARCA) Project," NUREG/CR-7008, U.S. Nuclear Regulatory Commission. Washington, DC. August, 2014.

15. J. Cardoni, "Radionuclide Inventory and Decay Heat Quantification Methodology for Severe Accident Simulations," SAND2014-17667, Sandia National Laboratories, Albuquerque NM, 2014.

16. Private Communication from M.T. Leonard to D.A. Kalinich, June 2012.

17. OECD-NEA Benchmark Study of the Accident at the Fukushima Daiichi NPS Project (BSAF Project), "Operational Data," Tokyo, Japan. November 6-8, 2012.

18. U.S. NRC, "Severe Accident Risks: An Assessment for Five U.S. Nuclear Power Plants – Final Summary Report", NUREG 1150, Vol. 1, U.S. Nuclear Regulatory Commission, Washington, D.C., 1990.

19. Oak Ridge National Laboratory, "Scale: A Comprehensive Modeling and Simulation Suite for Nuclear Safety Analysis and Design," ORNL/TM-2005/39, Version 6.1, June 2011. Available from Radiation Safety Information Computational Center at Oak Ridge National Laboratory as CCC-785.SCALE reference

20. TEPCO Plant Data, http://www.tepco.co.jp/nu/fukushima-np/plant-data/f1_3_Keihou3.pdf, accessed April 6 (2014).

21. Paul Bourke, http://paulbourke.net/fractals/

22. J. Cardoni and D. Kalinich, "Fukushima Daiichi Unit 1 Uncertainty Analysis – Preliminary Selection of Uncertain Parameters and Analysis Methodology," SAND2014-1170, Sandia National Laboratories, Albuquerque, NM, 2014.

23. M.R. Denman and D.M. Brooks, "Fukushima Daiichi Unit 1 Uncertainty Analysis – Exploration of Core Melt Progression Uncertain Parameters – Volume II," SAND2015-6612, Sandia National Laboratories, Albuquerque, NM, 2015.

24. American National Standard for Decay Heat Power in Light Water Reactors, ANSI/ANS-5.1-2005, American Nuclear Society (2005).

# DISTRIBUTION

Sandia National Laboratories